Study of Organic Light Emitting Transistors (OLETs)

A THESIS
SUBMITTED TO THE FACULTY OF THE GRADUATE SCHOOL
OF THE UNIVERSITY OF MINNESOTA
BY

Salil Tushar Bapat

IN PARTIAL FULFILLMENT OF THE REQUIREMENTS
FOR THE DEGREE OF
MASTER OF SCIENCE

C. Daniel Frisbie
Russell J. Holmes

December 2011

Contents

List of Figures

List of Tables

1 Introduction

1.1 *Introduction to Organic Semiconductors*

Semiconductors are materials that have conductivities in between metals and insulators.[1] Group IV Semiconductors like Silicon and Germanium and III-V compounds like Gallium-Arsenide and Gallium-Nitride are widely used for various electrical and optoelectronic applications. The semiconductor industry developed at a rapid pace during the last century with advent of devices like field effect transistors(FETs) and light-emitting diodes(LEDs). The use of organic materials as semiconductors has provided an interesting alternative to the costly processing associated with conventional semiconductor materials since Heeger[2] demonstrated that some polymers can show high electrical conductivity. Small molecules like Pentacene, as well as polymers like Poly-3-HexylThiophene(P3HT) are considered as organic semiconductors . These compounds generally have conjugated bonding which is believed to be useful to form a Pi cloud of electrons helping the conduction of charge carriers.[3] There are a few advantages to using organic semiconductors over inorganic semiconductors. Organic semiconductors can be processed at much lower temperatures as compared to inorganic semiconductors which require high purity, high temperature processing conditions. Organic materials consist of van der waals bonds and hence could be even deposited on a flexible substrate and can even just be printed[4] on a plastic substrate.[5] These properties make them ideal for the large area display applications as compared to their inorganic counterparts.

Light emission from organic crystals was reported in 1963 by Pope et al.[6]. But efficient light emission from a bi-layer structure of thermally evaporated organic thin films by Tang[7] was the key in development light emitting diodes from organic semiconductors. These light emitting diodes have been shown to work with very high luminescence efficiencies.[8] The emission wavelength can also be tuned by choosing a suitable dopant.[8] Along with light-

emitting diodes organic semiconductors were also shown to work as field-effect transistors. Horowitz et al[9] showed a field-effect transistor(FET) with α-conjugated sexithienyl (α-6T). Since then there has been a vast development in the area of OFETs. Over the years there has been considerable improvement in mobilities(μ) of OFETs through improving the device processing to alter film properties and also due to development of new materials.[10]

Although the basic construction of these devices is same as inorganic counterparts there are some inherent differences between organic and inorganic semiconductors. The charge transport in organic semiconductors is believed to be mainly due to hopping process as compared to band transport in inorganic semiconductors.[11] Organic semiconductors typically have π-conjugated system due to orbital overlap leading to delocalization of electrons and are generally described by molecular orbital picture.[11] The Highest Occupied Molecular Orbital (HOMO) state is equivalent to the top of a valence band and Lowest Unoccupied Molecular Orbital (LUMO) is equivalent to the bottom of a conduction band. Another major difference in these materials is that organic semiconductors mainly rely on charge injection from metal electrodes with suitable work functions unlike inorganic semiconductors where charge carriers are present either intrinsically or by virtue of doping. Majority of the research in this field is focused on improving the performance of organic light emitting diodes (OLEDs), organic field effect transistors (OFETs) and organic solar cells. Following sections give a general introduction to these devices followed by a brief motivation for the project.

1.2 *Introduction to Organic Field Effect Transistors*

1.2.1 Organic Field Effect Transistors (OFETs)

Organic field effect transistors have attracted a lot of attention in recent years for their potential application in the areas of large active matrix displays, novel devices made on flexible substrates and even as smart cards and ID tags.[10] Small molecule semiconductors like Pentacene[12], single crystals like Rubrene[13] and Tetracene[14] and also polymers like P3HT[15] have been demonstrated to work with charge carrier mobilities of the order of or even greater than 1 cm^2/V-s in a field effect transistor geometry. An OFET has the following important components.

1. Source-Drain Contacts
2. Active Organic Semiconductor layer
3. Gate dielectric
4. Gate contact

Depending on the spatial arrangement of these features 3 different architectures can be classified, with each having certain advantages and disadvantages. Figure 1 shows three different type of architectures with (c) being the most popular amongst the three due to its ease of fabrication. The length between the source and drain contact is known as channel length (as the channel of charge carriers forms between these two electrodes effectively). Channel width is defined as lateral extent on source-drain electrodes (Figure 2) .

1.2.2 Working of Organic Field Effect Transistors

The operation of an OFET is similar to those constructed from inorganic semiconductors.[16] The gate dielectric film works as a parallel plate capacitor. It is assumed that the electric field along the channel (parallel to the current flow direction) is much smaller than the

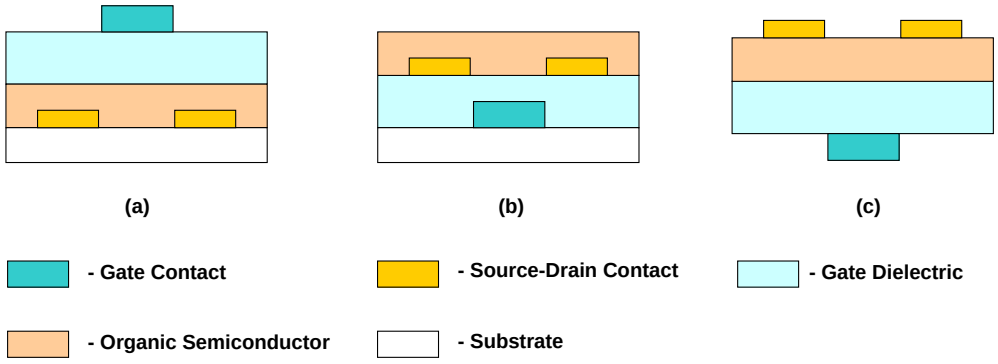

Figure 1: Standard OFET architectures
(a) Bottom Contact -Top gate architecture (b) Bottom contact - Bottom Gate architecture (c) Top Contact - Bottom Gate architecture

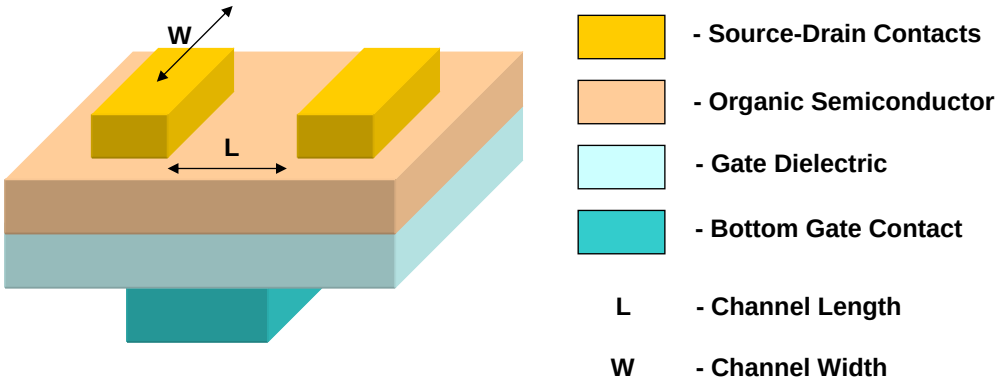

Figure 2: Schematic of a top-contact, bottom gate configuration.

electric field across the channel (perpendicular to the current flow direction).[17] This condition is generally satisfied when the channel length is much larger than the dielectric thickness and is known as 'gradual channel approximation'.[18] The applied voltage across the dielectric is responsible for accumulation of charges in the channel. When a voltage is applied across the channel (between source and drain electrodes) these carriers can move due to the applied electric field leading to current.[4] Under standard biasing conditions the source electrode is grounded, the drain voltage (V_D) is applied to the drain electrode and gate voltage (V_G) is applied to the gate electrode. Typical measurements include measuring the drain current (I_D) as a function of the gate voltage (V_G) at a constant drain voltage (V_D) (known as transfer characteristics) and the drain current (I_D) as a function of the drain voltage (V_D) at a constant gate voltage (V_G)(known as output characteristics). Carrier mobility (μ) is one important parameter which can then be calculated from these curves by using eq.1, where L, W, I_D, V_G, V_D are as defined above and C is the capacitance per unit area of the dielectric film.[19] Other important parameters include the transistor ON/OFF ratio which is the ratio of the current when the transistor is in on state(on current) to current when the transistor is in off state(off current) and threshold voltage(V_T). Threshold voltage is the voltage applied at which we have mobile charges in the channel.[19] This voltage generally has a non-zero value due to the effect of traps on the charge carriers and band bending due to energy level mismatch between organic semiconductor and the contact.[19] The effective applied voltage in the channel then is V_G-V_{Th}.

$$\mu = \frac{L}{W} \cdot \frac{\partial I_D}{\partial V_G} \cdot \frac{1}{C \cdot V_D} \tag{1}$$

During I_D-V_D sweep, at zero drain to source voltage, charges are uniformly distributed at the semiconductor-dielectric interface.[17] As the drain to source voltage (V_D) is increased, gradient of charge density is formed from the source electrode to the drain electrode.[17] This

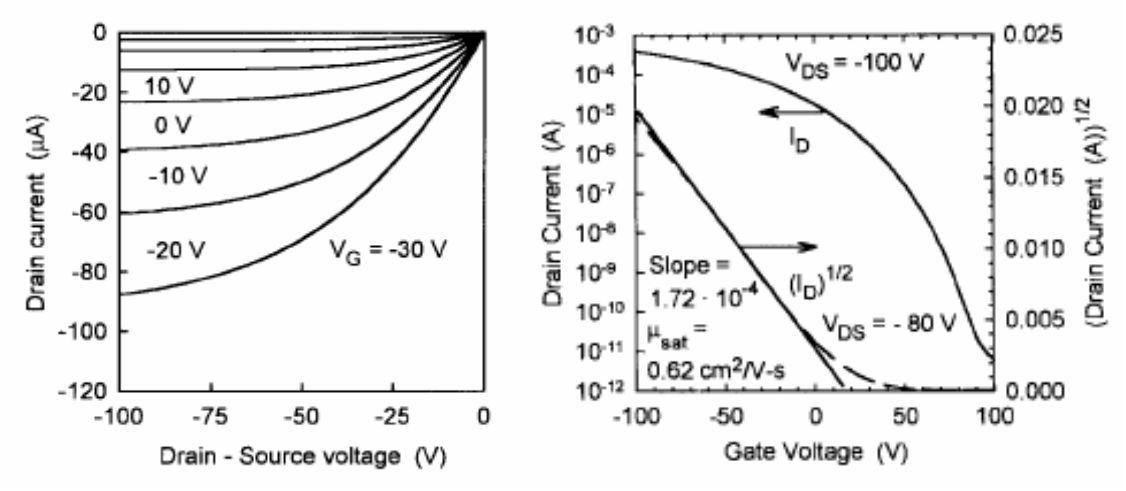

Figure 3: Output and Transfer Characteristics of Pentacene Transistor
(a) Output Curves and (b) Transfer Curves[20]

regime is known as linear regime as the current flowing increases linearly with V_D.[17],[19] As the drain to source voltage is increased further, at one point V_G becomes equal to V_D-V_{Th}, which is known as "pinch-off" point.[17] As V_D is increased further, a depletion region is formed near the drain electrode and the transistor goes into saturation.[19] Current does not increase further even though V_D is increased and carriers are swept across the depletion region by high electric field.[17],[19] During I_D-V_G sweep, initially there are no mobile carriers in the channel until V_G fills all the traps.[19] After gate voltage is increased further, mobile charges are introduced in the channel which are swept off across the channel resulting in current. The density of mobile charges varies linearly with V_G as seen from the transfer characteristics. Figure 3 shows typical transfer and output characteristics of an OFET.

1.3 *Short introduction to Organic-Light Emitting Diodes*

1.3.1 Organic Light Emitting Diodes (OLEDs)

Other interesting application of organic semiconductors is making of light emitting devices especially organic light emitting diodes (OLED). Tang[7] first showed a bi-layer OLED structure by using thermally evaporated thin films of small organic molecules. Later Burroughes et al[21] showed light emitting diodes with PolyPhenyl Vinylene type of polymers. Since then there has been a lot of improvement in these devices. Wide range of small molecules and polymers has been used in making good OLEDs. Different device architectures are being used for efficient LEDs these days. A very basic OLED has a transparent anode(generally Glass coated with Indium Tin Oxide), Hole Transport layer (HTL), Emissive layer(EML), Electron Transport layer(ETL) and a low work function(needed for electron injection) anode. Figure 4 shows the device structure and energy band diagram.

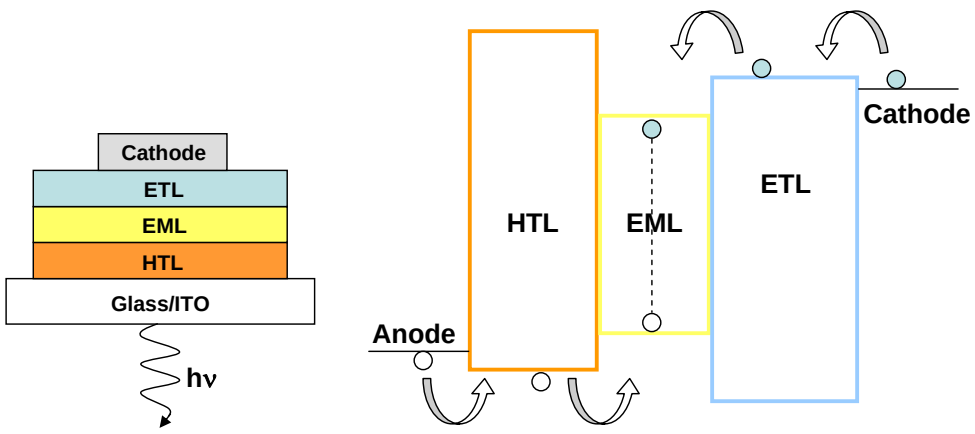

Figure 4: Basic OLED device structure

1.3.2 Working Principle of OLEDs

With application of electric field electrons are injected from the cathode and holes from the anode.[22] Lining up the energy level of these contacts with the adjoining layers is really important as it ensures efficient carrier injection into the device. Holes and electrons are then transported through HTL and ETL into EML. The energy level alignment of this emissive layer with HTL and ETL again plays an important role in terms of transfer. This type of alignment is necessary for carrier confinement[23] which leads to higher probability of radiative recombination. Electrons and holes in EML then form bound electron-hole pairs called excitons.[24] Separating EML from anode and cathode reduces the possibility of excitons getting annihilated at these electrodes. This effect is known as exciton quenching[25] and is non-radiative in nature thus reducing the efficiency of the device. Excitons thus formed in EML then emit light upon radiative recombination, the exact nature of which depends on excited state properties of EML and quantum mechanical selection rules.[22] Optimization of the device structure is necessary to ensure charge balance which contributes to efficient light emission.[26] The final efficiency of the device depends on all these factors and the actual way to collect the emitted light.[8]

1.4 *Motivation*

As stated above both OFETs and OLEDs have been widely studied. A typical organic display would then consist of OLEDs with OFETs making up the circuitry needed to drive the display. An idea of combining both transistors and light-emitting characteristics gave rise to a novel concept known as light emitting transistors. The basic idea is to have a transistor with organic material which can emit light. Light emission form a transistor near the source electrode has been observed in Tetracene single crystal transistors.[27], [28] The light emission in these devices has been reported to be because of excitons forming near the electrode. The device in itself only conducts one carrier type (either holes or electrons) and due to the electric field close to the electrode, other type of carriers are tunneled in to form excitons which then radiate the light out. This is briefly depicted in Figure 5 . As the exciton formation takes place near one of the electrodes there is a strong chance that excitons might decay by non-radiation means such as exciton quenching as described is previous section.

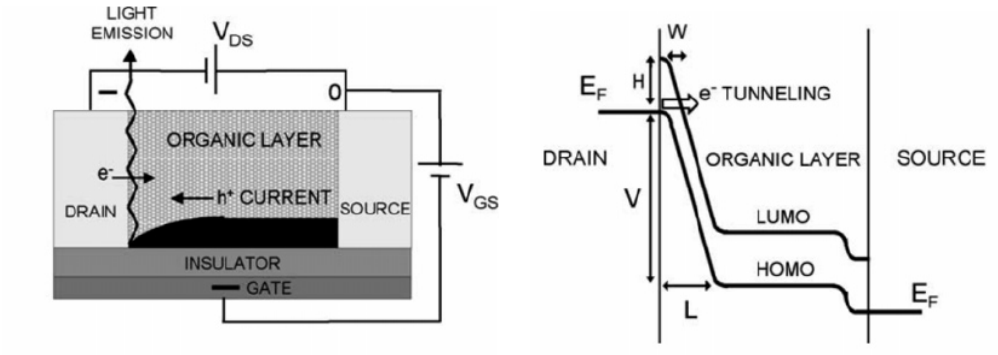

Figure 5: Schematics of light emission from Tetracene
(a)Device structure and (b)corresponding energy band diagram[27]

The restriction of light emission only near the electrodes of unipolar device suggests

that we should instead use an ambipolar material. In such a case both electron and hole accumulation layers could be achieved at the same time in the transistor channel, and the exciton recombination zone would be in the middle of the channel and not near the contact electrodes thus reducing the problems with exciton quenching. This will be discussed in more detail in chapter 2.

More efficient OLEDs are being reported these days with the use of luminescent dopants after Tang et al[31] demonstrated that separating the functions of charge transport and light emission on two different molecules can lead to more efficient devices. In these devices, dopant which can either be phosphorescent or fluorescent is in a host matrix such that exciton formed on the host is transferred to the dopant. This method then allows us to tune the wavelength of light emission by changing the dopant. Energy transfer in OLEDs has been successfully employed to get efficient devices with different colors. The concept of energy transfer has been discussed in more detail in the next chapter. The same idea can potentially be applied to these light-emitting field effect transistors(OLET). The idea of using energy transfer in these devices then will allow us to separate the functions of ambipolar transport and light emission to two different molecules. Although light-emitting FETs have been shown there are not many materials which can work as ambipolar OLETs. Due to scarcity of good ambipolar light-emitting materials, we are also limited to very few emission wavelengths. Using luminescent dopants in OLETs is a possible alternative that might lead to expansion of emission wavelengths.

Chapter 2 provides a review of important concepts including theory of ambipolar transistors, light emission from organic materials and key concepts behind energy transfer. Chapter 3 is focussed on brief discussion of experimental techniques involved followed by discussion of results. Ambipolar transistors fabricated using Pentacene, a blue light emitting small

molecule BSBP and green light emitting polymer F8BT as active materials are reported.

References

[1] B. G. Streetman and S. K. Banarjee, *Solid State Electronic Devices* (Pearson Education, 2007).

[2] A. J. Heeger, Faraday Discussions of the Chemical Society **88**, 202 (1989).

[3] J. M. Shaw and P. F. Seidler, IBM Journal of Research & Developement **45**, 3 (2001).

[4] Z. Bao, J. A. Rogers and H. E. Katz, Journal of Material Chemistry **9**, 1895 (1999).

[5] Z. Bao and J. J. Locklin, editors, *Organic field-effect transistors* (CRC Press).

[6] M. Pope, H. P. Kallmann and P. Magnante, The Journal of Chemical Physics **38**, 2042 (1963).

[7] C. W. Tang and S. A. VanSlyke, Appl. Phys. Lett. **51**, 913 (1987).

[8] D. Ammermann, A. Böhler and W. Kowalsky, Annual report 1995, Institut für Hochfrequenztechnik, TU Braunschweig , 48 (1995).

[9] G. Horowitz, D. Fichou, X. Peng, Z. Xu and F. Garnier, Solid State Communications, Vol. 72, No. 4, pp. 381-384, 1989. **72**, 381 (1989).

[10] C. D. Dimitrakopoulos and D. J. Mascaro, IBM Journal of Research & Developement **45**, 11 (2001).

[11] M. C. J. M. Vissenberg, *Opto-Electronic Properties of Disordered Organic Semiconductors*, PhD thesis, University of Leiden, 1999.

[12] T. Minari, T. Nemoto and S. Isoda, J. Appl. Phys. **96**, 769 (2004).

[13] V. C. Sundar, J. Zaumseil, V. Podzorov, E. Menard, R. L. Willett, T. Someya, M. E. Gershenson and J. A. Rogers, Science **303**, 1644 (2004).

[14] J. H. Schön, Synth. Met. **122**, 157 (2001).

[15] A. Tsumura, H.Koezuka and T.Ando, Appl. Phys. Lett. **49**, 1210 (1986).

[16] D. A. Neamen, *Semiconductor Physics and Devices* (McGraw-Hill, 2007).

[17] J. Zaumseil and H. Sirringhaus, Chem. Rev **107**, 1296 (2007).

[18] G. Horowitz, Adv. Mater. (Weinheim, Ger.) **10**, 365 (1998).

[19] C. R. Newman, C. D. Frisbie, D. A. da Silva Filho, J.-L. Brédas, P. C. Ewbank and K. R. Mann, Chemical Materials **16**, 4436 (2004).

[20] D. Gundlach, Y. Lin, T. Jackson, S. Nelson and D. Schlom, IEEE Electron Device Letters **18**, 87 (1997).

[21] J. H. Burroughes, D. D. C. Bradley, A. R. Brown, R. N. Marks, K. Mackay, R. H. Friend, P. L. Burns and A. B. Holmes, Nature **347**, 539 (1990).

[22] Z. Li and H. Meng, editors, *Organic light-emitting materials and devices* (Taylor and Francis, 2007).

[23] A. Dodabalapur, Solid State Commun. **102**, 259 (1997).

[24] J. R. Sheats, H. Antoniadis, M. Hueschen, W. Leonard, J. Miller, R. Moon, D. Roitman and A. Stocking, Science,New Series **273**, 884 (1996).

[25] Z.H.Kafafi, editor, *Organic Electroluminescence* (Taylor and Francis, 2005).

[26] L. S. Hung and C. H. Chen, Materials Science and Engineering R **39**, 143 (2002).

[27] A. Hepp, H. Heil, W. Weise, M. Ahles, R. Schmechel and H. von Seggern, Phys. Rev. Lett. **91**, 157406 (2003).

[28] C. Santoto, R.Capelli, M.A.Loi, M.Murgia, F. Cicoira, V.A.L.Roy, P.Stallinga, R.Zamboni, C.Rost, S.F.Karg and M.Muccini, Synth. Met. **146**, 329 (2004).

[29] J. Zaumseil, C. Donley, J. Kim, R. Friend and H. Sirringhaus, Adv. Mater. (Weinheim, Ger.) **18** (2006).

[30] T. Sakanoue, M. Yahiro, C. Adachi, H. Uchiuzou, T. Takahashi and A. Toshimita, Appl. Phys. Lett. **90**, 171118 (2007).

[31] C. W. Tang, S. A. VanSlyke and C. H. Chen, J. Appl. Phys. **65**, 3610 (1989).

2 Review of Concepts

2.1 *Ambipolar Light Emitting Field Effect Transistors*

2.1.1 Ambipolar transistors

An ambipolar semiconductor can transport both holes and electrons efficiently.[1] Inorganic semiconductors are inherently ambipolar as they have both holes and electrons present by virtue of doping. Similarly, one would expect pure organic semiconductors to also show ambipolar behavior in OFETs because of their intrinsic nature.[2] But, in practice, organic semiconductors generally show only p-type or n-type behavior. However ambipolar transistors have been realized in practice by using two separate materials working as n-type and p-type separately. Primarily these types of devices have either blended or bi-layer heterostructure types of architecture. Table 1 summarizes a few such devices that have been reported so far.

However, the idea of using two different semiconductors is not that useful for good light emitting FETs. Using a single material that is ambipolar is much more desirable as it reduces the complexity, eases the processing of the device and may simplify the use of suitable guest molecule.[10] Cornil et al have looked at the theoretical aspects charge transport through organic materials indicating that intrinsically organic semiconductor should transport both holes and electrons efficiently.[11] Hence, observed unipolar operation of organic materials can be attributed external factors rather than intrinsic factors. Before examining working of single component ambipolar devices we first need to understand some important factors that need to be considered for getting ambipolar operation in single component transistors. There are four important factors which should be considered while designing an ambipolar transistor as discussed below.

1. **Gate Dielectric:** It is observed that organic semiconductors predominantly behave

No.	Materials Used	Reported Data	Ref.
1	poly(benzobisimidazobenzophenanthroline) (BBL) and poly(10-hexylphenoxazine-3,7-diyl-alt-3-hexyl-2,5-thiophene) (POT) or poly[(thiophene-2,5-diyl)-alt-(2,3-diheptylquinoxaline-5,8-diyl)] (PTHQx)	Blend Concentration dependent	[3]
2	α-quinquethiophene (α-5T) and N,N'-ditridecylperylene-3,4,9,10-tetracarboxylic diimide (P13)	$\mu_h = 10^{-4} cm^2$/V-s $\mu_n = 10^{-3} cm^2$/V-s	[4], [5]
3	Pentacne and N,N'-ditridecylperylene-3,4,9,10-tetracarboxylic diimide (PTCDI-$C_{13}H_{27}$)	μ_h=0.09 cm^2/V-s $\mu_n = 9.3 \times 10^{-3} cm^2$/V-s	[6]
4	5,5'-bis(4-biphenylyl)-2,2'-bithiophene (BP2T) and C_{60}	-	[7]
5	dihexyl-quaterthiophene (DH4T) and N,N'-ditridecylperylene-3,4,9,10-tetracarboxylic diimide (P13)	$\mu_h = 0.03 - 0.002 cm^2$/V-s $\mu_n = 0.03 - 0.04 cm^2$/V-s	[8]
6	Pentacene and tris(8-quinolinolato)aluminum (Alq3)	$\mu_h = 2.1 \times 10^{-3} cm^2$/V-s	[9]

Table 1: Reported two component ambipolar transistors

as p-type materials and achieving n-type transport has proven to be a tough task. It is believed that the dangling -OH bonds present at the SiO_2-semiconductor interface are responsible for trapping electrons and preventing them from moving through the transistor channel. Thus it is important to have a dielectric which will not trap electrons due to the dangling bonds. One way of achieving this is to use some kind of buffer layer over SiO_2 layer. This buffer layer can be a thin film of a metal (e.g. Cr [12]), a polymer film (e.g. PMMA [13]), or an alkene layer (e.g. n-triacontane [14]). The other alternative is to use polymer film as gate dielectric solely instead of SiO_2 as reported in case of F8BT.[15] The advantage of using a polymer dielectric is that it does not have any inherent trap sites, but it can be difficult to get a polymer film without defects which leads to increased current leakage.

2. **Contacts:** An ambipolar transistor must have both holes and electrons in the channel. Since charge is injected through the metal contacts, it then becomes imperative that the source and drain contacts are selected so that one injects holes into the channel while other injects electrons. As the difference between the HOMO (or LUMO) and the work function of the metal contact increases the contact resistance also goes up and carrier injection becomes less efficient. It is thus necessary that the energy levels of the contacts are well matched with the organic semiconductor so that there is facile injection of both electrons and holes. Using symmetric contacts(source and drain contacts are the same material) might not be useful even though it is much simpler to realize in practice. Hence it is also necessary to have the semiconductor such that its HOMO and LUMO levels lie fairly close with the work functions of some of the metals used as contacts. Sakanoue et al report symmetric Al contacts[13] with BSBP as semiconductor and later have used angled evaporation technique to get asymmetric Al and Au contacts with BSBP-C6 as semiconductor.[16] They report that

using asymmetric contacts improves the device performance.[16] Whereas Zaumseil et al used Au as their contacts with F8BT as semiconductor.[15] Energy level of Au falls exactly in the middle of the F8BT band gap and thus injects both holes and electrons.[15]

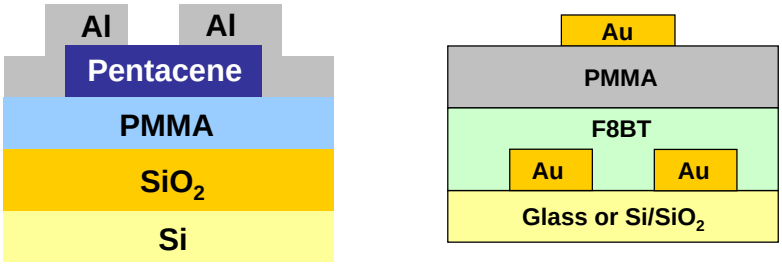

Figure 6: Pentacene and F8BT ambipolar device architecture

3. **Device Architecture:** As discussed in Section 1.2.1 we can have different device architectures for OFETs with each having its own set of advantages and drawbacks. Figure 6 shows the device architectures used for ambipolar pentacene and F8BT devices. Top contact-bottom gate architecture is easy to work with and generally has Si/SiO_2 as a substrate which requires use of a buffer layer as described above thus increasing one step. For bottom contact-top gate architecture we can as well use glass as substrate and use polymer dielectric which will not trap electrons. This has been successfully employed for making ambipolar transistor with F8BT by Zaumseil et al.[15] The carriers are not only injected from the sides of source drain electrode but also from all those areas where the gate electrode overlaps with the source-drain electrodes which leads to "Current Crowding" effect. [1] The contact resistance is reduced due to this effect and thus we have efficient injection of charge carriers.

4. **Environmental Conditions:** In addition to all the factors described above we also

need to consider the effect of processing conditions and the environment on these devices. It is observed that n-type behavior is generally very sensitive to oxygen and moisture in the air. Hence, it is necessary that all the processing and even device testing should be done in inert atmosphere in order to observe ambipolar behavior.

Zaumseil et al[15] have used a polyfluorene material Poly(9,9-di-n-octyl-fluorene-alt-benzothiadiazolo) (F8BT) exclusively for making OLETs, while Sakanoue et al[13] have used a small molecule 4,-4'-bis(styryl)biphenyl (BSBP) for making blue light emitting FETs. Table 2 summarizes ambipolar FETs with a single semiconductor layer reported so far.

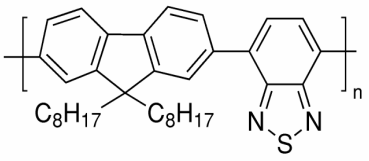

(a) Poly(9,9-di-n-octyl-fluorene-alt-benzothiadiazole), F8BT

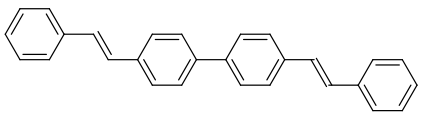

(b) 4,-4'-bis(styryl)biphenyl, BSBP

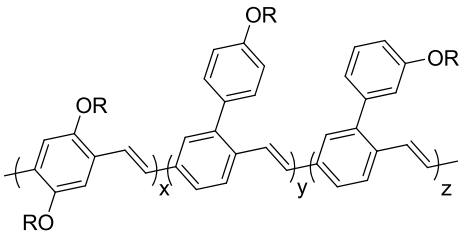

(c) Aryl-substituted poly(p-arylene vinylene), Super Yellow

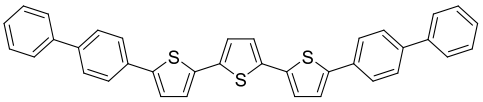

(d) α,ω-bis(biphenyl-4-yl)-terthiophene, BP3T

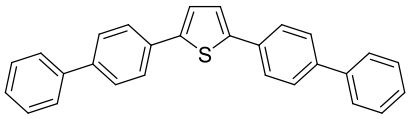

(e) 2,5-bis(4-biphenylyl)thiophene, BP1T

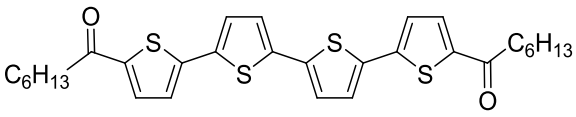

(f) R,ω-dihexylcarbonylquaterthiophene, DHCO-4T

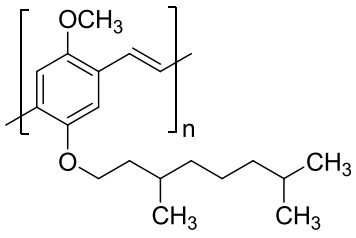

(g) Poly(2-methoxy-5-(3,7-dimethyloctoxy)-p-phenylenevinylene), MDMO-PPV

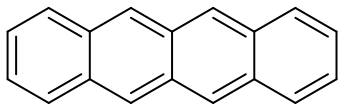

(h) Tetracene

Figure 7: Molecules used to make ambipolar devices

No.	Material	Device Processing	Reported Data	Ref
1	F8BT Fig.7(a)	Solution Processing Bottom contact-Top gate Au Source-Drain contacts PMMA as gate dielctric	$\mu_h = 7 - 9 \times 10^{-4} cm^2$/V-s $\mu_n = 7 - 9 \times 10^{-4} cm^2$/V-s	[15]
2	BSBP Fig. 7(b)	Thermal Evaporation Top Contact-Bottom Gate Al Source-Drain Contacts PMMA as Buffer layer	$\mu_h = 1.5 \times 10^{-3} cm^2$/V-s $\mu_n = 2.5 \times 10^{-5} cm^2$/V-s	[13]
3	SuperYellow Fig. 7(c)	Solution Processing Top Contact-Bottom Gate Ca-Au, Ca-Ag Asymmetric contacts PPcb, PbTTT as Buffer layer	$\mu_h = 2.1 \times 10^{-5} cm^2$/V-s $\mu_n = 1.5 \times 10^{-5} cm^2$/V-s	[17] and [18]
4	BP3T Fig. 7(d)	BP3T Top Contact-Bottom Gate Al:Li and Au asymmetric contacts n-triacontane as buffer layer	$\mu_h = 9.13 \times 10^{-3} cm^2$/V-s $\mu_n = 2.94 \times 10^{-2} cm^2$/V-s	[14]
5	BP1T Fig. 7(e)	BP1T Top Contact-Bottom Gate Au or Pt Source Drain Contacts	-	[19]
6	DHCO-4T Fig. 7(f)	DHCO4T Top Contact-Bottom Gate SAM or PVA or PMMA buffer layer Cu, Au, Ag, Ca used for contacts	Various mobilities for devices with different contacts	[12]
7	BP3T Fig. 7(d)	BP3T single crystal Top Contact-Bottom Gate Au-Ca asymmetric contacts	-	[20]
8	MDMO-PPV Fig. 7(g)	MDMO-PPV Bottom Contact-Bottom Gate Au-Ca asymmetric contacts BCB as buffer layer	-	[21]
9	Tetracene Fig. 7(h)	Tetracene single crystal Top Contact-Bottom Gate Au-Mg asymmetric contacts PMMA as buffer layer	$\mu_h = 4.3 \times 10^{-2} cm^2$/V-s $\mu_n = 1 \times 10^{-2} cm^2$/V-s	[22]

Table 2: Reported single component ambipolar transistors

2.1.2 Ambipolar transistor device operation

Figure 8 schematically shows the operation of a bottom contact OLET. The working of OLET is similar to a standard organic FET as described in section 1.2.2. The main difference is that both the electrodes now inject charge carriers into the channel region as depicted in figure 8.

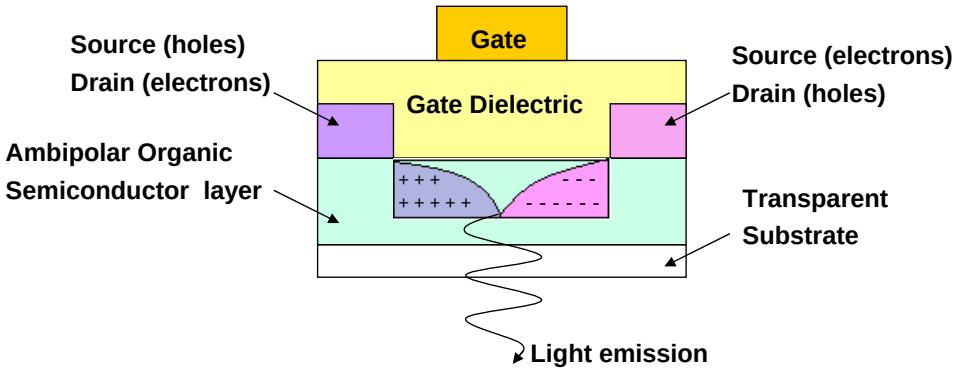

Figure 8: Schematic of bottom contact OLET illustrating formation of holes and electron accumulation layers and light emission

In the case of an ambipolar transistor, we can have both holes and electrons in the transistor channel region depending on the biasing conditions. It should be noted here that both holes and electrons are not present at all biasing conditions. The conventional drain defined with respect to electrons is actually source for holes and vice versa. Source electrode injects electrons into the channel when the potential difference between gate and source electrode is more that the threshold voltage for electron injection. Similarly, holes are injected when potential difference between gate and drain electrode is greater than the threshold voltage for injection of holes. Ambipolar transfer characteristic of an ambipolar

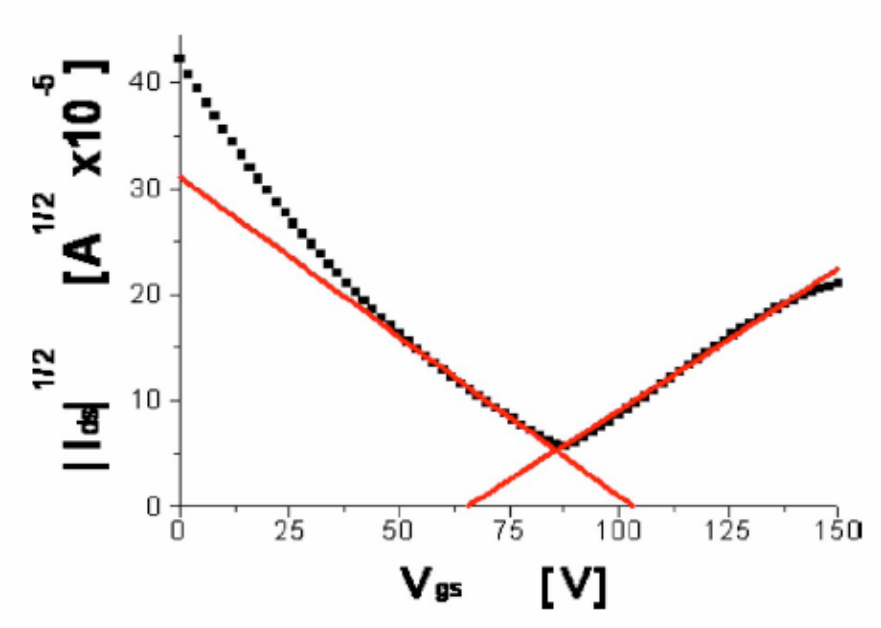

Figure 9: Transfer characteristics of ambipolar transistor
Taken from [17]

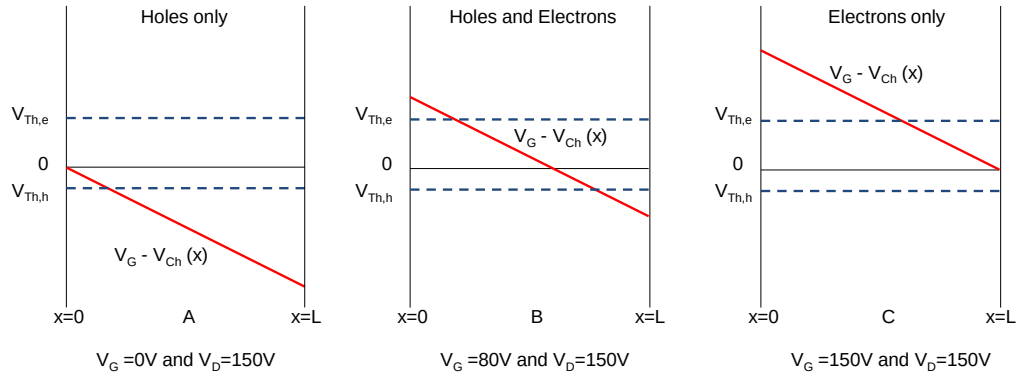

Figure 10: Simplified schematic of effective channel potential in ambipolar transistor at different biasing conditions

transistor is depicted in the figure 9.[17] In this report, the source-drain voltage is kept at 150 V and gate voltage is swept from 0 to 150 V. As applied drain voltage is positive which is usually the case for n-type operation of transistor,source electrode is source for electrons and drain electrode will inject holes in the transistor. This can be easily understood by assuming liner voltage drop between source and drain electrodes then plotting a line representing V_G-$V_{channel}$ in the channel region as shown in fig.10. This assumption of liner voltage drop is just for the sake of simplicity and understanding will not be exactly valid in real case. Also x=0 is near the source electrode and x=L in near the drain electrode where L is the channel length. Initially, when the gate voltage V_G is small, the potential difference between source and gate is less than the threshold voltage for electrons but holes are being injected as the potential difference between the drain electrode and gate is larger than threshold for holes as seen in fig.10(A). As the gate voltage is increased further, at voltage near 80 V, the threshold voltage for electrons is exceeded and we are still above threshold voltage for holes as seen in fig.10(B). At this point, both electrons and holes are being injected into the channel. This is the ambipolar working regime of the transistors. After increasing the gate voltage further, we reduce the potential difference between gate and drain electrode below the threshold for holes and thus stopping injection of holes in the channel. Referring to fig.10 it can be said that increasing the drain voltage will increase the slope of channel potential line and thus will increase the range of ambipolar operation. Changing the gate voltage during the sweep moves the channel potential line up and down and changing the extent of charge injection.

Several variations have been tried in order to make these devices better and to understand the device physics in ambipolar transistors. Naber et al have incorporated a high-k dielectric in F8BT ambipolar devices in order to get higher currents in these devices.[23] Zaumseil et al have also studied the effect of morphology of F8BT film. Amorphous film shows

more continuous light emission than polycrystalline films.[24] It is argued that this is due to anisotropic mobility along different direction in F8BT film[24]. When the film is aligned parallel to the charge transport direction light emission is more intense.[25] Quantum efficiencies for these light emitting transistor devices have also been reported in these reports. Even though quantum efficiencies of $\sim 0.55\%$ in F8BT devices[26] and $\sim 0.15\%$ in SuperYellow devices[18] have been reported, standardizing a fixed method to calculate efficiencies in ambipolar OLETs is necessary. Several groups have also tried to model the charge transport and light emission characteristics in OLETs which is the topic of the next section.

2.2 *Organic Electroluminescence and analysis*

2.2.1 Organic Light Emitting Diodes

Organic light emitting devices have acquired a lot of commercial interest after the development of efficient OLEDs. This section concentrates on the mechanism of light emission from organic molecules and will look more deeply into the energetics of these molecules. Most of the theory has been developed for the working of OLEDs but the theory can be extended to the case of OLETs. Section 1.3.2 describes a very simple device structure of an OLED and its operation. This part will cover the basics of light emission and is aimed towards defining some of the standard concepts used in the literature. Before probing into the details of light emission through organic devices it is necessary that we define some of the terms and concepts explained below:

Singlet and Triplet excited states: The excitons formed can be thought of as a collection of two electrons.[27] The four possible combinations of the wavefunctions (ψ) are: i) both spins up, ii) both spins down, iii) symmetric linear combination of one spin up and other spin down and iv) anti-symmetric linear combination of one spin up and other spin down.[27] These can be represented by following equations :

$$\psi = \frac{1}{\sqrt{2}}\{\uparrow(1)\downarrow(2) - \downarrow(1)\uparrow(2)\} \tag{2}$$

$$\psi = \frac{1}{\sqrt{2}}\{\uparrow(1)\downarrow(2) + \downarrow(1)\uparrow(2)\} \tag{3}$$

$$\psi = \uparrow(1)\uparrow(2) \tag{4}$$

$$\psi = \downarrow(1)\downarrow(2) \tag{5}$$

Equation 2 shows the wavefunction which is anti-symmetric (S=0) and is known as the singlet excited state. Equations 3, 4 and 5 describe the triplet states of the system which have net S=1 and are symmetric with respect to particles 1 and 2.

Fluorescence: Fluorescence is the radiation of light when the singlet excited state decays to the ground state.[28] It is generally very fast(shorter lifetime) as compared to phosphorescence.

Phosphorescence: Phosphorescence is the radiative decay of the triplet state to the ground state.[28] This has a higher lifetime than that of fluorescence.

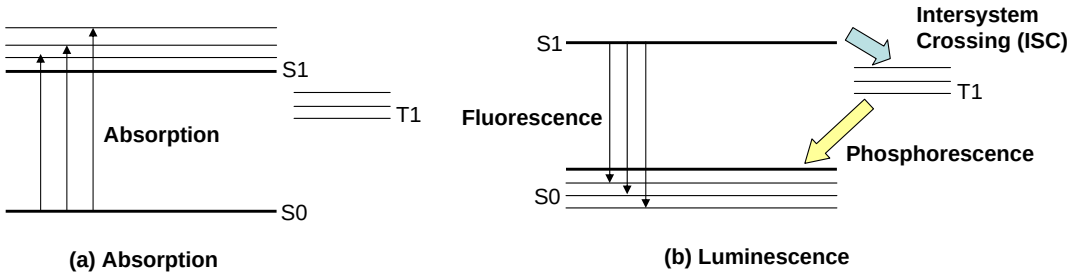

Figure 11: Energetics of organic molecule
Based on reference[29]

Dodabalapur[29] has explained the energetics of light emission in an organic molecule which is shown in figure 11. Due to their amorphous nature, organic molecules have discrete vibrational and rotational levels instead of bands as in inorganic semiconductors. After the molecule is excited, it relaxes to other vibrational states by non-radiative transitions and then relaxes to the ground state either by fluorescence or phosphorescence.[30] Due to these relaxations the emission wavelength is generally longer than absorption wavelength and the emission spectrum is usually shifted towards higher wavelength with respect to absorption spectrum.[29] This shift is known as Stokes shift. In a standard multi-layer OLED system as described in section 1.3.2 we have injection of charges from the anode and cathode which travel under the influence of an electric field to meet inside the EML.[31] In the EML electrons and holes combine to form an excited state.[32] Depending on whether the emitter is phosphorescent or fluorescent it then undergoes radiative decay to give out light.

This phenomenon is called electroluminescence because it is the electric field between the two electrodes that drives the carriers in the device to make them combine to emit light. The emission efficiency of these devices is usually low. Current systems use the host-guest system where a host molecule transfers the exciton to a guest molecule which has higher emission efficiency.

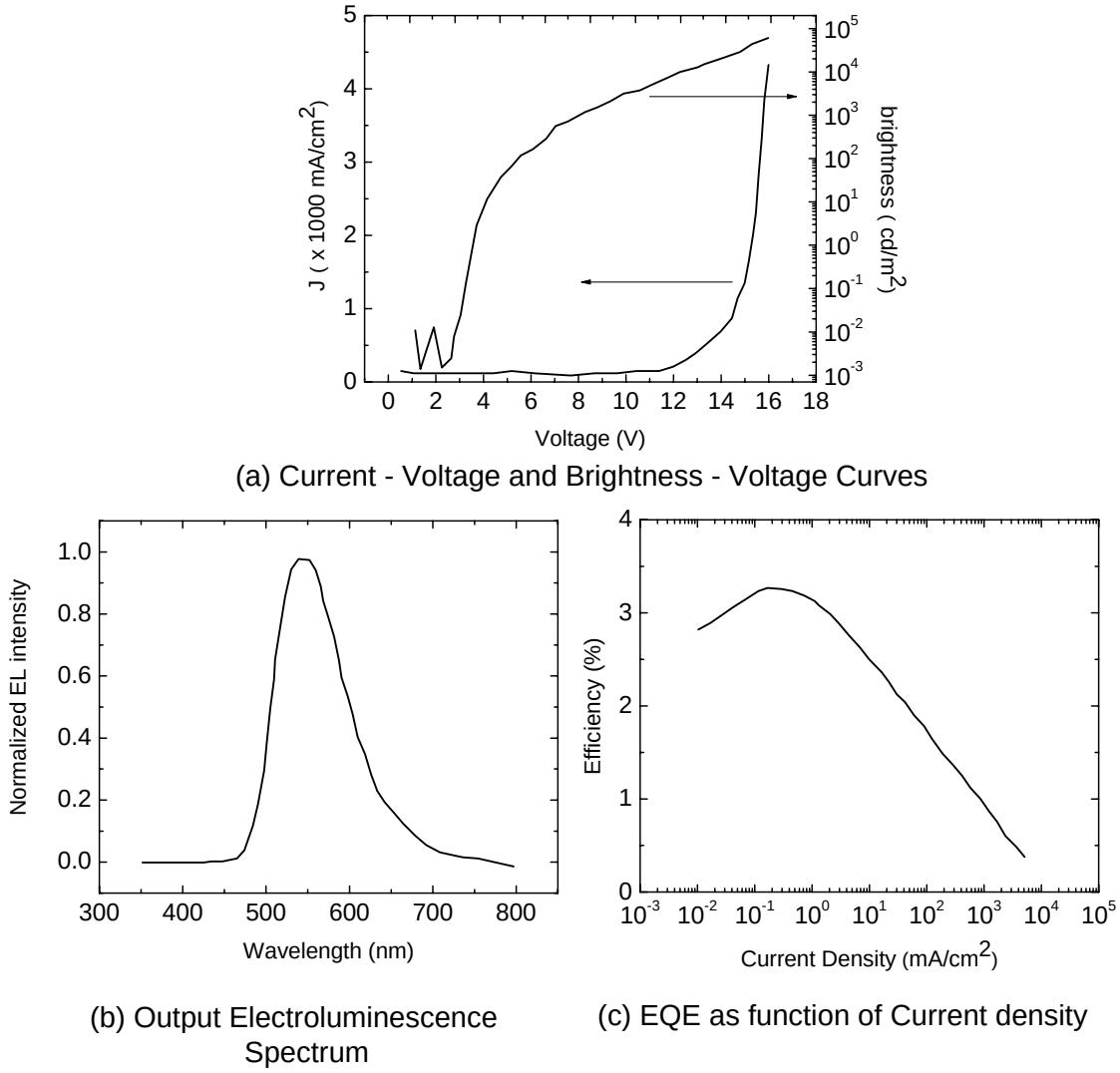

Figure 12: Typical OLED measurement data and analysis
Taken from [33]

A typical OLED is characterized by its Current Density (J)-Voltage(V) and Brightness-Voltage(V) curves. From these curves and the output wavelength spectrum we can then calculate External Quantum Efficiency (EQE). Figure 12 shows the data obtained for DFBTA green emitting OLED with new HTL material synthesized and tested by Yu Ku et al.[33] Figure 12(a) shows the variation of brightness with respect to voltage and the current voltage (J-V) curve which resembles to that of a diode. Figure 12(b) shows the output spectrum of the OLED which clearly shows that intensity peaks around 540 nm indicating that the emission is green. Figure 12(c) shows the EQE as variation of current density. As it can be seen from the diagram the maximum efficiency obtained for the device is about 3.2%. The decrease in efficiency with increase in current has been attributed to opening of other non-radiative pathways like exciton quenching and singlet-polaron quenching. The exciton dynamics and quenching mechanisms in OLETs is not completely understood and needs to be studied.

2.2.2 Efficiency Calculations

Organic electroluminescent devices are characterized by their efficiencies. Quantum efficiency is defined as ratio of photons generated per number of electrons injected into the device.[29] As described in section 1.3.2, a few of the important factors that affect the device efficiency are: balanced charge injection, carrier confinement to reduce quenching effects, and an optimized device geometry which is needed to ensure that emitted light can be collected in high yield. A detailed analysis of the losses involved and efficiency calculations is provided below.Internal quantum efficiency (η_{int}) and external quantum efficiency (η_{ext}) are defined by following equations[34] where χ is spin fraction, η_{PL} is the fraction of singlet excitons

that undergo radiative decay and η_{OC} is outcoupling efficiency.[34]:

$$\eta_{int} = \gamma \cdot \chi \cdot \eta_{PL} \tag{6}$$

$$\eta_{ext} = \gamma \cdot \chi \cdot \eta_{PL} \cdot \eta_{OC} \tag{7}$$

γ is the ratio of the number of excitons formed to the number of injected electrons. If there is balanced charge injection in the device then γ tends to unity.[34] As seen in the last section, an exciton formed can be either a singlet exciton or a triplet exciton. There are three possible wavefunction combinations that lead to triplet excited states while there is only one such combination for singlet excited state. Thus in general we are expected to have 75% triplet excitons and 25% singlet excitons.[35] Transitions from singlet spin state to singlet ground state are allowed but transitions from the triplet excited state to the singlet ground state are not allowed because of spin conservation. Transitions from the triplet to the singlet ground state are non-radiative and are not efficient.[35] The factor χ thus takes care of singlet-triplet ratio. Out of these excited state singlet not all decay radiatively to the ground state. Other non-radiative mechanisms such as thermal deactivation compete with fluorescence. Extent of these mechanisms decides the value of η_{PL}. By proper choice of materials and their thicknesses, fluorescence can become a dominant mechanism making η_{PL} closer to unity. Apart from these device structure and device physics criteria, there are some limitations in terms of light collection. Typically in an OLED structure, we have light emission from the top or bottom of the device depending on the device structure. However there is also a possibility that light will be emitted from the sides of the glass substrate due to internal reflections. These losses along with Fresnel losses in organic films are grouped together into efficiency factor η_{OC}. These are roughly estimated to be $\sim$11-15%.[32]

As seen above, the singlet-triplet ratio is one important factor that hampers the efficiency

of the device which can be improved. It was shown that there are some materials which can exhibit decay from the triplet state to the singlet ground state accompanied by light emission. Such materials are known as phosphorescent materials. Advancements in the field of OLEDs for improving device performance have been brought by efficient use of phosphorescent materials and with energy transfer. The idea of energy transfer is explained in detail in the next section. Apart from these improvements, efficiency can further increased by changing the device structure in order to reduce outcoupling losses of the device. Designing hemispherical or dome shaped substrates[32], or the use of optical microcavities[34] could reduce optical losses and improve the device performance. These loss mechanisms and exciton dynamics will affect efficiencies in OLETs as well.Understanding exciton physics and improving device efficiencies is a part of current research on OLETs.

2.3 *Review of Energy Transfer*

2.3.1 Motivation

As seen in previous section, the singlet to triplet ratio of excitons generated in an OLED device is 1:3. Fluorescence from singlet excited states is quantum mechanically permitted and phosphorescence is a disallowed transition. Hence, in general, only singlet excitons will be able to decay radiatively and triplet excitons will not. However it was observed that by inducing heavy metal complexes triplet states can be made to decay radiatively. This will improve the device efficiency by reducing non-radiative losses. One more issue with OLEDs is that a good emitter molecule may not always have good transport properties. So it is beneficial if we split the functions of charge transport and emission to two different species.[36] By choosing suitable host molecules and guest molecules we can improve the device performance. If there is an efficient phosphorescent molecule as the guest with compatible host molecule efficiency can be improved. The basic idea of energy transfer is to have guest molecules(either phosphorescent or fluorescent) in a matrix of host molecules (typically fluorescent). The physics of energy transfer is explained in detail in next section followed by its applications in the field of OLEDs.

2.3.2 Physics of Energy Transfer

Before going further into the details of energy transfer in organic materials the following terms are defined.

Host: The molecule in the OLED device on which charges combine to form an exciton is called as host. Thus it is important that host should have good transport properties.

Guest: The guest accepts the exciton formed on the dopant molecule through energy transfer. However it is also possible in some systems that an guest molecule may

trap charges and form an exciton.

Spin-Orbit Coupling: The intermixing of singlet and triplet states caused due to spin flips caused by the magnetic field generated within the material is termed as spin-orbit coupling.[37] Heavier metal atoms have more nuclear charge and as a result have strong spin orbit coupling.[37] Spin-orbit coupling is very important factor to consider in phosphorescent devices.

Having described some key concepts above we can now describe important energy transfer mechanisms.

1. **Cascade Transfer:** Cascade transfer is the simplest energy transfer mechanism. During cascade transfer, the exciton formed on the host decays radiatively and the light is absorbed by the guest forming an exciton on the guest. This exciton then undergoes radiative decay to emit light.[37] The overall effect due to fluorescence and reabsorption within the material itself is to increase the effective lifetime of the singlet fluorescence.[38] For reabsorption to happen, there should be overlap in the fluorescence spectrum of the host and the absorption spectrum of the guest.

2. **Förster Transfer:** Förster transfer is a long-range transfer process which can be thought as coulombic exchange or induced dipole interaction process.[37][38] Förster transfer needs spin conservation and hence the transfer from a singlet host to a triplet guest is not possible with Förster transfer.[39] Like cascade transfer process, Förster transfer also requires overlap between the luminescence spectrum of host and the absorption spectrum of the guest is necessary.[38] In Förster transfer mechanism, unlike cascade energy transfer, fluorescence from the host does not occur, but instead the relaxation of host excited state is coupled with absorption in the guest.[40] In other words, there exists a Coulombic interaction between the host excited state electron and the guest ground state electron which causes the coupling between host and guest.[37]

Figure 13 depicts this type of energy transfer. Considering that the coupling is due to dipole-dipole interaction between host and guest we can formulate the rate constant for this type of energy transfer. The equation which governs the rate constant of Förster energy transfer can be written as in eq.8 where k is the constant, κ^2 accounts for the interaction between two dipoles, $J(\varepsilon_A)$ is similar to the overlap integral, and R_{DA} is the distance between two dipoles.[37] The averaged value of κ^2 constant is 2/3. The efficiency is directly proportional to $(\frac{R_0}{R_{DA}})^6$ where R_0 is the critical distance between host and guest at which excitation of guest and relaxation of host have equal probability and is given by eq.9.

$$k_{ET} = k\frac{\kappa^2 k_D^o}{R_{DA}^6} J(\varepsilon_A) \tag{8}$$

$$\eta = \frac{1}{\tau_s}(\frac{R_0}{R_{DA}})^6 \tag{9}$$

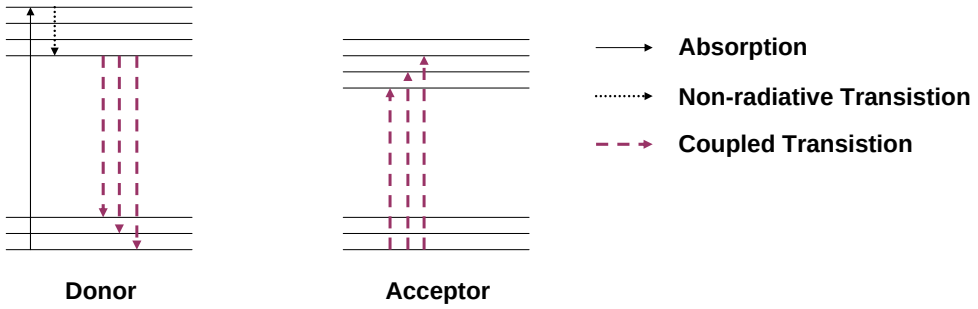

Figure 13: Schematic of Förster Transfer
Based on [40]

3. **Dexter Transfer:** Dexter transfer is a short-range transfer process which occurs through electron exchange between the host and the guest. It is different from Förster

transfer in the sense that there is physical transfer of the electrons between host and guest.[37] The constraint on this type of transfer is conservation of the total spin. Hence triplet to triplet transfer is feasible with this mechanism.[41] When two molecules are very close to each other, their electron clouds overlap and then electron transfer is made possible.[37] The process can be visualized with the help of figure 14. D* and A* denote excited states of host and guest respectively. The probability of energy transfer can be expressed by equation 10.[38] The β_{DA} term denotes the exchange interaction term between the host and guest molecules.[42] The integral represents the effective density of states (ρ_{eff}). The rate constant for the energy transfer is given by equation 11 where K represents orbital interactions, J is overlap integral, R_{DA} is the distance between guest and host and L denotes van der Waals radii.[37] The exponential dependence comes from the fact that the interaction between two molecules varies exponentially with distance.

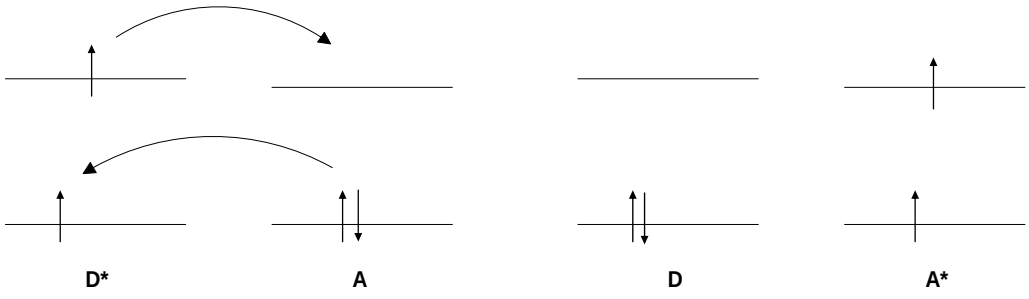

Figure 14: Schematic of Dexter Transfer
Based on [37]

$$K_{D\to A} = \frac{2\pi}{\hbar}|\beta_{DA}|^2 \int F_D(E)F_A(E)dE \tag{10}$$

$$k_{ET} = KJe^{(-2R_{DA}/L)} \tag{11}$$

With a clear idea of the possible mechanisms of energy transfer we now look at the different processes which are important in the host-guest OLED system. Relative rate constants of various species help in determining the dominant mechanism of transfer and the properties of radiation. Depending on whether we have phosphorescent host(guest) or fluorescent host(guest) several processes may take precedence over the others. It is thus necessary to know the key processes in host-guest systems:

- **Triplet energy transfer:** Triplet energy transfer generally occurs via a Dexter transfer process. It can be summarized by Equation 12.[27]

$$^3D^* + {}^1A \to {}^1D + {}^3A^* \tag{12}$$

- **Singlet energy transfer:** Singlet energy transfer is possible by both Dexter and Förster transfer but due to its long-range nature Förster transfer generally dominates with lower guest concentration. It can be summarized by Equation 13.[27]

$$^1D^* + {}^1A \to {}^1D + {}^1A^* \tag{13}$$

- **Triplet-Singlet energy transfer:** Triplet state to singlet energy transfer is also possible by Förster transfer. It is called sensitized fluorescence and is shown by Equation 14.[27]

$$^3D^* + {}^1A \to {}^1D + {}^1A^* \tag{14}$$

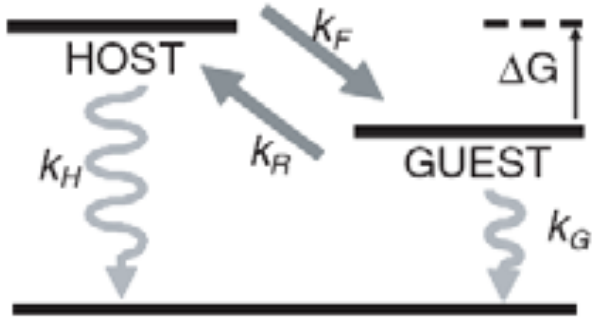

Figure 15: Energy dynamics of Host-Guest system
Taken from [27]

- **Inter-System Crossing:** It is essential for good phosphorescent materials that excitons transferred to singlet states also get transferred to triplet states.[41] The process in which an electron is exchanged between a singlet excited state and a triplet excited state is known as inter-system crossing(ISC).[43] This process is assisted by spin-orbit coupling and occurs with the flipping of spin.[44] This process differs from internal conversion where there is no spin inversion and the transfer takes place either from singlet to singlet or from triplet to triplet.[44] Both these processes are non-radiative processes.

Baldo and Segal explain four important factors which should be considered for good host-guest systems as shown in figure 15. The four important rate constants to consider are, the decay of the guest excited state (k_G), the decay of host excited state(k_H), the forward(k_F) and the reverse(k_R) transfer rates between the host excited state and the guest excited state. The guest phosphorescence can be maximized either by having $k_G \gg k_H$

or $k_F \gg k_R \gg k_H$.[45] If the host is phosphorescent and has a large decay lifetime first condition is satisfied and efficient guest phosphorescence is achieved. The second condition is useful in endothermic (ΔG>0) cases (guest triplet level higher that host triplet level) in order to have a sufficient population of excitons on guest triplet state.[45] These factors play important role in deciding the host and guest materials in organic light emitting devices.

With the idea of having fluorescent or phosphorescent dopants in the OLED structure numerous things have been tried in order to design OLED systems with higher efficiency and to control the emission wavelength (color) of these devices. Lots of effort has been concentrated on getting efficient white OLEDs. Both fluorescent[36] and phosphorescent dopants[39] have been reported. With more understanding of the device physics, a variety of different dopants have been tried in order to get light of different colors. As seen in previous discussion, using efficient phosphorescent guests which typically have a heavy metal ion, light emission occurs from triplet states which improves efficiency of OLEDs. Thus, energy transfer to suitable dopants is the key in getting efficient OLEDs with desired emission wavelength. Organic LEDs are more suitable for display or lighting applications which do not require the spatial control.[46] White light emitting devices require molecules that emit in Red, Blue and Green. This also is achieved by incorporating two or more dopants in a suitable host material. Same idea can potentially be applied in organic light emitting transistors.

References

[1] J. Zaumseil and H. Sirringhaus, Chem. Rev **107**, 1296 (2007).

[2] N. Karl, Synthetic Metals **133-134**, 649 (2003).

[3] A. Babel, Y. Zhu, K.-F. Cheng, W.-C. Chen and S. A. Jenekhe, Adv. Funct. Mater. **17**, 2542 (2007).

[4] C. Rost, S. Karg, W. Riess, M. A. Loi, M. Murgia and M. Muccini, Appl. Phys. Lett. **85**, 1613 (2004).

[5] M. A. Loi, C. Rost-Bietsch, M. Murgia, S. Karg, W. Riess and M. Muccini, Adv. Funct. Mater. **16**, 41 (2006).

[6] K. N. N. Unni, A. K. Pandey, S. Alem and J.-M. Nunzi, Chem. Phys. Lett. **421**, 554 (2006).

[7] K. Yamane, H. Yanagi and S. Hotta, Thin Solid Films **516**, 3157 (2008).

[8] F. Dinelli, R. Capelli, M. A. Loi, M. Murgia, M. Muccini, A. Facchetti and T. J. Marks, Adv. Mater. (Weinheim, Ger.) **18**, 1416 (2006).

[9] C. an Di, G. Yu, Y. Liu, X. Xu, D. Wei, Y. Song, Y. Sun, Y. Wang and D. Zhu, Adv. Funct. Mater. **17**, 1567 (2007).

[10] M. Mas-Torrent and C. Rovira, Chemical Society Reviews **37**, 827 (2008).

[11] J. Cornil, J.-L. Brédas, J. Zaumseil and H. Sirringhaus, Adv. Mater. (Weinheim, Ger.) **19**, 1791 (2007).

[12] R. Capelli, F. Dinelli, S. Toffanin, F. Todescato, M. Murgia, M. Muccini, A. Facchetti and T. J. Marks, Journal of Physical Chemistry **112**, 12993 (2008).

[13] T. Sakanoue, M. Yahiro, C. Adachi, H. Uchiuzou, T. Takahashi and A. Toshimita, Appl. Phys. Lett. **90**, 171118 (2007).

[14] K. Yamane, H. Yanagi, A. Sawamato and S. Hotta, Appl. Phys. Lett. **90**, 162108 (2007).

[15] J. Zaumseil, C. Donley, J. Kim, R. Friend and H. Sirringhaus, Adv. Mater. (Weinheim, Ger.) **18** (2006).

[16] T. Sakanoue, M. Yahiro, C. Adachi, J. H. Burroughes, Y. Oku, N. Shimoji, T. Takahashi and A. Toshimitsu, Appl. Phys. Lett. **92**, 053505 (2008).

[17] J. S. Swensen, J. Yuen, D. Gargas, S. K. Buratto and A. Heeger, J. Appl. Phys. **102**, 013103 (2007).

[18] E. B. Namdas, P. Ledochowitsch, J. D. Yuen, D. Moses and A. Heeger, Appl. Phys. Lett. **92**, 183304 (2008).

[19] T. Yamao, Y. Shimizu, K. Terasaki and S. Hotta, Adv. Mater. (Weinheim, Ger.) **20**, 4109 (2008).

[20] S. Z. Bisri, T. Takenobu, Y. Yomogida, T. Yamao, M. Yahiro, S. Hotta, C. Adachi and Y. Iwasa, Proceedings of SPIE **6999**, 69990Z (2008).

[21] H. Sirringhaus, J. Zaumseil and R. Friend, Nat. Mater. **5**, 69 (2006).

[22] T. Takahashi, T. Takenobu, J. Takeya and Y. Iwasa, Adv. Funct. Mater. **17**, 1623 (2007).

[23] R. C. G. Naber, M. Bird and H. Sirringhaus, Appl. Phys. Lett. **93**, 023301 (2008).

[24] J. Zaumseil, R. J. Kline and H. Sirringhaus, Appl. Phys. Lett. **92**, 073304 (2008).

[25] J. Zaumseil, C. Groves, J. M. Winfield, N. C. Greenham and H. Sirringhaus, Adv. Funct. Mater. **18**, 3630 (2008).

[26] J. Zaumseil, C. R. McNeill, M. Bird, D. L. Smith, P. P. Ruden, M. Roberts, M. J. McKiernan, R. H. Friend and H. Sirringhaus, J. Appl. Phys. **103**, 064517 (2008).

[27] M. Baldo and M. Segal, physica status solidi (a) **201**, 1205 (2004).

[28] M. Segal, M. Singh, K. Rivoire, S. Difley, T. V. Voorhis and M. A. Baldo, Nat. Mater. **6**, 374 (2007).

[29] A. Dodabalapur, Solid State Commun. **102**, 259 (1997).

[30] G. F. Barlow and K. A. Shore, J. Mod. Opt. **47**, p1921 (20000915).

[31] J. R. Sheats, H. Antoniadis, M. Hueschen, W. Leonard, J. Miller, R. Moon, D. Roitman and A. Stocking, Science,New Series **273**, 884 (1996).

[32] D. Ammermann, A. Böhler and W. Kowalsky, Annual report 1995, Institut für Hochfrequenztechnik, TU Braunschweig , 48 (1995).

[33] S.-Y. Ku, L.-C. Chi, W.-Y. Hung, S.-W. Yang, T.-C. Tsai, K.-T. Wong, Y.-H. Chen and C.-I. Wu, J. Mater. Chem. **19**, 773 (2009).

[34] L. S. Hung and C. H. Chen, Materials Science and Engineering R **39**, 143 (2002).

[35] S. Kappaun, C. Slugovc and E. J. W. List, International Journal of Molecular Sciences **9**, 1527 (2008).

[36] C. W. Tang, S. A. VanSlyke and C. H. Chen, J. Appl. Phys. **65**, 3610 (1989).

[37] N. Turro, *Modern Molecular Photochemistry* (University Science Books, 1991).

[38] M. Pope and C. E. Swenberg, *Electronic Processes in Organic crystals and Polymers*, Second ed. (Oxford Science Publications, 1999).

[39] M. A. Baldo, D. F. O'Brien, Y.You, A. Shoustikov, S. Sibley, M. E. Thompson and S. R. Forrest, Nature **395**, 151 (1998).

[40] T. Förster, Discussions of Faraday Society **27**, 7 (1959).

[41] M. A. Baldo, M. E. Thompson and S. R. Forrest, Pure Appl. Chem. **71**, 2095 (1999).

[42] D. L. Dexter, The Journal of Chemical Physics **21**, 836 (1953).

[43] H.Yersin, editor, *Highly Efficient OLEDs with Phosphorescent Materials* (Wiley-VCH, 2008).

[44] M. Klessinger and J. Michl, *Excited States and Photochemistry of Organic Molecules* (VCH Publishers, 1995).

[45] M. A. Baldo and S. R. Forrest, Physical Review B **62**, 10958 (2000).

[46] Z.H.Kafafi, editor, *Organic Electroluminescence* (Taylor and Francis, 2005).

3 Experimental Techniques

This section provides details of the experimental techniques used and transistor measurement tools.

3.1 *Sample Preparation*

The devices were fabricated on two types of substrates : i) 3000$\mathring{A}$ SiO_2 thermally grown on a Si wafer and ii) glass substrates. Substrate cleaning helps to remove any impurities or dust particles that might hamper device performance. A standard procedure for cleaning involves the following steps.

1. 5 min sonication in alkaline soap solution and DI water
2. 5 min sonication with DI (deionized) water
3. 5 min sonication with Acetone (2 times)
4. 5 min rinse with boiling Isopropyl Alcohol(IPA)
5. Blow dry with Nitrogen
6. Repeat boiling IPA clean and blow dry
7. 10 min exposure to UV-Ozone

Clean substrates were then transferred to a nitrogen glovebox for the deposition of organic materials and metal contacts. Polymers were deposited by spin coating while other small molecules and metals were thermally evaporated over the substrate. Details of each system are provided in the next section.

3.2 *Deposition Techniques and Characterization*

3.2.1 Thermal Evaporation

Small molecules (e.g. pentacene) and metals are deposited by a thermal evaporation system present inside the nitrogen glovebox. Figure 16 shows the thermal evaporator. All thermal evaporations are done in vacuum with pressure $< 2 \times 10^{-6}$ torr. Processing the materials under vacuum is important to avoid oxidation of materials at their melting temperatures. Two pumps are used to create the vacuum. A mechanical (roughing) pump is used to evacuate the chamber to low vacuum and then a cryogenic (cryo) pump provides high vacuum. The evaporator system has 2 organic furnaces (O1 and O2) for organic evaporations and two metal posts (M1 and M2) for metal evaporations. During evaporation current is passed through metal posts/organic furnace to heat up a boat/furnace. Two thermocouples monitor the temperature of organic furnace while a current controller measures the current passing through the metal posts. Cooling water runs through the furnace/posts and to the substrate holder to control temperature and prevent overheating. The current is increased slowly and after the temperature inside the furnace reaches the sublimation temperature of organic material, it starts to sublime. For metals, increasing current melts the metal and then evaporation starts. The rate of evaporation is monitored by quartz crystal microbalance (QCM) crystals and is read by the QCM crystal monitor outside. Substrate temperature can also be controlled by separate heating wires. Substrate heating can alter the morphology of the film which plays a very important role in determining the charge transport properties of the semiconductor. The samples are mounted on a substrate holder with the desired shadow masks covering the samples fixed by the help of clips. Shadow masking allows us to pattern the source-drain electrodes and organic semiconductors as desired for a given device geometry. A shutter is used to cover (closed position) the sample substrate until the desired evaporation rate is obtained. The shutter is moved aside (open position) after the desired rate is obtained. Vacuum is not broken(venting

the chamber) until the organic furnace temperature drops down below 60°C in case of organic evaporation. In case of metal evaporations, vacuum is broken after waiting for 30 min after the evaporation. This is necessary in order to prevent oxidization of materials being used.

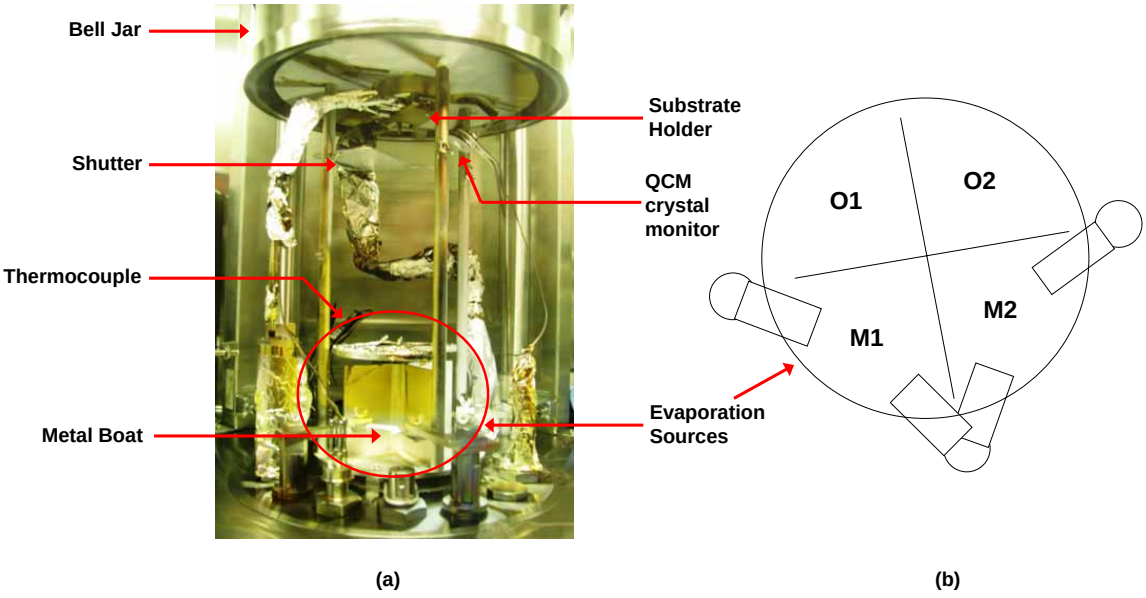

Figure 16: Thermal evaporation system
(a) Photograph and (b) Schematic of evaporation sources

3.2.2 Spin Coating

Spin coating is a technique which is generally employed for depositing thin films of polymers from solutions. In spin coating, the sample is mounted on the chuck and is held in place by vacuum. The solution is then dropped on the sample and sample is then revolved at a high rotation rate for a certain time(generally 1 min). Part of the solid and all of the solvent is expelled radially from the substrate leaving a thin film of the remaining solid of interest. To alter the morphology, sample is often annealed at a certain temperature above the glass

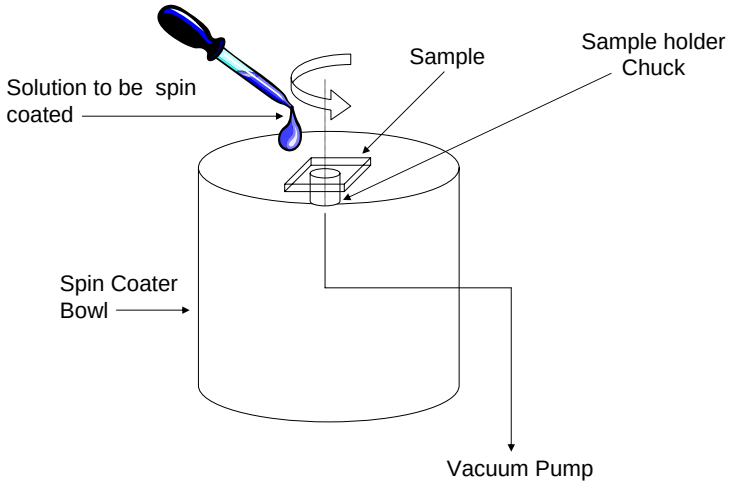

Figure 17: Schematic of Spin Coater

transition temperature on a hotplate inside the glovebox. Figure 17 shows a schematic of spin coater.

3.2.3 Characterization

The devices were characterized by the use of spectroscopic ellipsometer. Ellipsometer was used to determine all the thickness measurements of deposited layer. The technique of ellipsometry measurements can be briefly summarized as follows.

The standard thickness measurement using ellipsometer involves deposition of a thin film at identical growth conditions as to the actual experiment on a Silicon wafer of known thickness. Ellipsometry is a non-destructive technique used to determine thickness and optical constants for the material.[2] It is based on the measurement of the relative change in the phase of polarized light beam after reflection from the thin film.[1] Ellipsometry uses elliptically polarized light which can be described by x and y components of electric field of light traveling in z-direction as shown in figure 18. For elliptically polarized light these

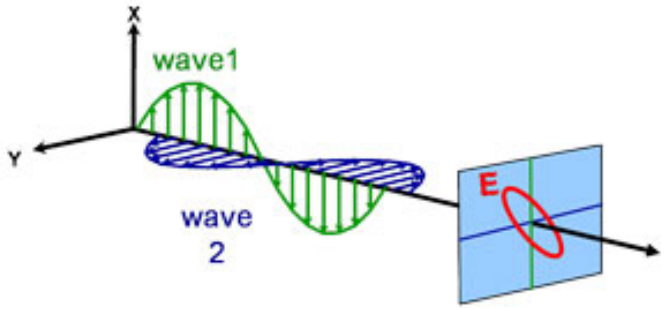

Figure 18: Elliptically polarized light
[1]

two linearly polarized components are combined out of phase by some angle.[3] When this angle is 90° we have circularly polarized light.

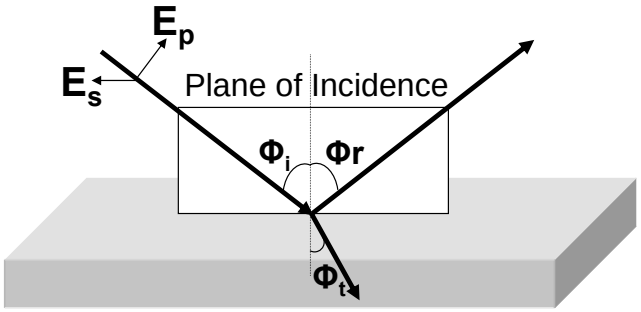

Figure 19: Light incident on a film showing p and s components of the electric field and plane of incidence

Taken from [3]

$$r_s = (\frac{E_{0r}}{E_{0i}})_s = \frac{n_i \cos(\phi_i) - n_t \cos(\phi_t)}{n_i \cos(\phi_i) + n_t \cos(\phi_t)} \quad r_p = (\frac{E_{0r}}{E_{0i}})_p = \frac{n_t \cos(\phi_i) - n_i \cos(\phi_t)}{n_i \cos(\phi_t) + n_t \cos(\phi_i)}$$

$$t_s = (\frac{E_{0t}}{E_{0i}})_s = \frac{2n_i \cos(\phi_i)}{n_i \cos(\phi_i) + n_i \cos(\phi_t)} \quad t_p = (\frac{E_{0t}}{E_{0i}})_p = \frac{2n_i \cos(\phi_i)}{n_i \cos(\phi_t) + n_t \cos(\phi_i)} \tag{15}$$

Figure 19 depicts a polarized light wave interacting with an interface. Light is partially transmitted and partially reflected. The electric field can be divided in two components, parallel polarized component (p-component) and perpendicular polarized component (s-component), as shown in figure 19. Reflected light and transmitted light can again be split into p and s components of electric field. Applying boundary conditions for electric field along s and p directions provide solutions for these components of light reflected (r_p,r_s) and light transmitted (t_p,t_s) as per equation 15.[1] In the case of multiple films standard reflection and transmission equations written for a fabry-perot cavity can be applied.[4] The complex refractive index($\tilde{n}$), which includes the refractive index(n) and the extinction coefficient(k) as optical constants can be defined by equation 16.[1]

$$\tilde{n} = n + ik \tag{16}$$

$$\Delta = \delta_1 - \delta_2 \tag{17}$$

$$tan\psi = \frac{|R^p|}{|R^s|} \tag{18}$$

$$\rho = \tan\psi e^{i\Delta} \tag{19}$$

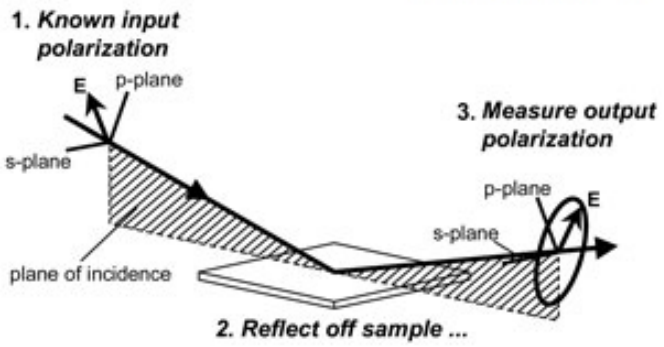

Figure 20: Experimental setup used for ellipsometry measurements
Taken from [1]

Figure 20 represents the experimental setup used for ellipsometry that consists of a light source, polarization generator, sample, polarization analyzer, and detector.[1] Two parameters that are measured during ellipsometry are Δ and ψ defined by equations 17 and 18, where δ_1,δ_2 are phase difference between the p and s waves before and after reflection respectively and R^p,R^s are ratios of amplitudes of outgoing wave and incoming wave respectively for p and s waves.[3] The fundamental equation for change in polarization(ρ) in ellipsometry measurement can be written as equation 19.[1] After carrying out the measurements, optical constants and film thicknesses can be extracted by fitting constructed models with experimental data. A model is first constructed which describes the sample layers.[1] Initial guesses for the parameters are then given to the data analysis tool which then fits the model with experimental data following regression analysis.[1] Parameters are then extracted after the mean square error(MSE), which quantifies difference between fits and experimental data, is minimized.[1] The measurements can be carried out at multiple wavelengths and different angles and are very sensitive to thickness of layers.[2] This technique can also be applied to multi-layered films to successfully obtain individual layer thicknesses.

3.3 *Measurement and Analysis*

The completed transistor devices were then tested inside a vacuum probe station shown in figure 21. The probe station setup consists of 2 power sources (Keithley 236 and Keithley 237 Source measure units) that are used to apply the gate voltage and the drain voltage. Two current measurement units (Keithley 2137A) are used to monitor the current.

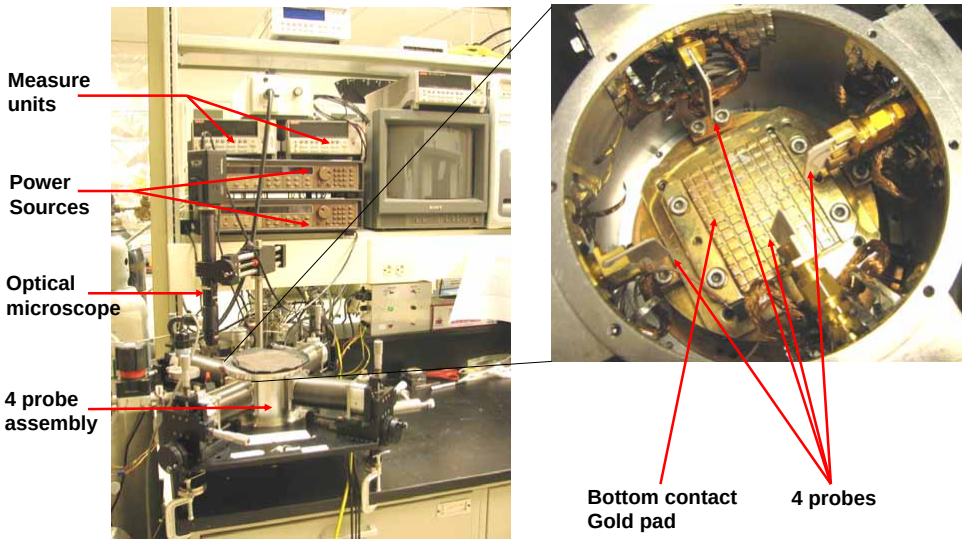

Figure 21: Photographs showing vacuum probe station setup

During the standard measurement, gold probes are used to make contact between the voltage source and device electrodes. The probe gently touches the electrodes which can be seen with the help of a microscope and display screen assembly. In the case of the bottom gate structure the contact through the bottom is made with the help of gold platform on which the device rests. After the contacts are made both transfer characteristics and output characteristics are measured. For transfer characteristics, the gate voltage is swept keeping the drain voltage constant, while to measure output characteristics drain voltage is swept keeping the gate voltage constant. The data points are collected at regular intervals of

voltage as per defined step voltage size.

Device characteristics are analyzed by plotting transfer curves and output curves. From the slope of saturation region of I_D-V_G plots(Transfer characteristics), $\frac{\partial I_D}{\partial V_G}$ can be extracted, which is used to calculate mobility using eq.1 for known transistor parameters including channel length and width.

References

[1] Light and materials- part 1, Online Resource, Ellipsometry tutorial.

[2] J. N. Hilfiker and R. A. Synowicki, Solid State Technology **39**, p157 (19961001).

[3] H. G. Tompkins and W. A. McGahan, *Spectroscopic ellipsometry and reflectometry : A users guide* (Wiley Interscience, 1999).

[4] A. Yariv, P. Yeh and P. Yeh, *Photonics: Optical Electronics in Modern Communications* (Oxford University Press, 2006).

4 Ambipolar Transistors using Pentacene and BSBP

4.1 *Introduction*

Pentacene has been a benchmark organic semiconductor and is one of the most studied small molecule organic semiconductor. Most of the research on Pentacene so far has been focused on p-type Pentacene transistors and single crystals. Over the past few years research has expanded to focus on making n-type and ambipolar transistors using Pentacene.[1][2] Recently, there have been reports of ambipolar transistor with Pentacene as active semiconductor using Aluminum contacts in order to achieve efficient injection of holes and electrons.[3] Ambipolar transistors using Pentacene were thus made following a similar approach and studied. Transistors were also fabricated in a tri-layer geometry using Pentacene and another small molecule in order to study injection and charge transport in tri-layer ambipolar devices.[4] Light emitting transistors using another small molecule 4,-4'-bis(styryl) biphenyl(BSBP) have been reported which use a similar top contact geometry as Pentacene ambipolar transistors.[5] BSBP is a wide band gap semiconductor and shows blue colored light emission. BSBP transistors were fabricated using the same approach as reported, however they show large threshold voltage(V_T) as compared to the reported values.[5] In order to further characterize these devices and to understand the cause of large V_T we also carried out AFM measurement on BSBP transistors.

4.2 *Experimental details*

Si wafer substrates with 3000$\mathring{A}$ of thermally grown SiO_2 were cleaned as per procedure described previously and silver paint was applied on the bottom as bottom gate contact. A 15 mg/ml solution of PMMA (mol.wt. 350k) was prepared with 1,2 Di-chloroethane as a solvent and was stirred overnight at room temperature. PMMA was spin coated at 4500 RPM for 1 min in the Nitrogen glovebox and was baked for 1 hour at 120°C to get rid of the remaining solvent. PMMA thickness was measured to be 950 $\mathring{A}$ using Ellipsometry. Samples were then transferred to a thermal evaporator without air exposure. Pentacene obtained from H.W.Sands chemicals was used as received without any further purifications.350$\mathring{A}$ thick Pentacene films were deposited in the evaporator with the chamber pressure below 2×10^{-6} torr. Substrate temperature was kept at 60°C in order to improve the crystallinity of film. The growth rate was maintained in between 0.1-0.2 $\mathring{A}$/s. 1000$\mathring{A}$ Aluminum contacts were then deposited at 3 $\mathring{A}$/s as top source-drain electrodes. Two different shadow masks were used to pattern the semiconductor layer and the source-drain contacts. Channel width and length for Pentacene ambipolar transistors were 3000 μm and 30 μm respectively. BSBP transistors follow similar device processing steps as ambipolar Pentacene transistors. 350$\mathring{A}$ BSBP was evaporated at 0.1-0.2 $\mathring{A}$/s on PMMA coated SiO_2 substrates. The channel length and width for BSBP transistors was 30 μm and 3000 μm respectively. Fig.22 shows the energy level picture and device geometry of the devices fabricated with Pentacene and BSBP. The energy band diagram displays the work function of Aluminum roughly lies in the middle of the band gap of Pentacene and BSBP. This energy level alignment of metal contact work function is necessary to ensure injection of both holes and electrons in the channel. All transistors were tested in a vacuum probe station in inert atmosphere glovebox without any air exposure.

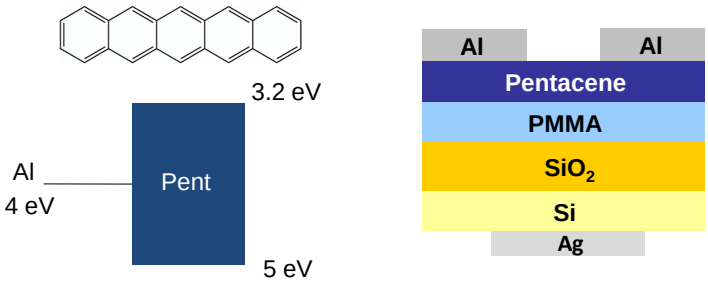

(a) Ambipolar Pentacene device structure with energy band diagram showing work function alignment of Al contact

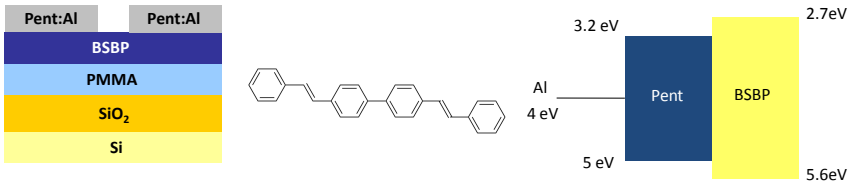

(b) Ambipolar BSBP device structure with energy band diagram showing work function alignment of Al contact

Figure 22: Device architectures and energy band diagram for BSBP and Pentacene ambipolar transistors

4.3 *Results and discussion*

4.3.1 Pentacene transistors

As shown in fig.23 Pentacene transistors exhibit clear ambipolar transfer characteristics on both p and n sides of applied gate voltage. These curves display V-shaped transfer characteristics typical of ambipolar transistors. The source current (I_S) and drain current(I_D) match well with each other confirming low gate leakage. When the drain voltage was varied the transfer curves showed increase in hole current for positive drain voltages and increase in electron current for negative drain voltages as seen in fig.24. In ambipolar transistors electrons and holes are injected from separate contacts. When transistors is operated at negative Gate and Drain voltage holes are injected from "Source" electrode while electrons are injected from "Drain" electrode.[6] Hence, when the negative applied Drain voltage is increased as shown is fig 24(a) it increases the electron current as shown while the hole current remains the same. Similarly when operated at positive Gate and Drain voltage, electrons are injected from "Source" electrode and holes are injected from "Drain" electrode. Fig.24(b) shows effect of increasing positive Drain voltage and as explained it shows increase in hole current while the electron current remains unchanged. This also results in the shift of "neck" point of the V-shaped curve as seen in the figure.

Charge carrier mobility is an important parameter that can be extracted from the transistor measurements. Linear charge carrier mobility was extracted by using mobility equation described previously. Electron and hole mobilities of Pentacene transistors was calculated from individual p-side and n-side transfer curves obtained at low applied drain voltages as depicted in fig.25. The hole mobility in these devices is 5×10^{-2} cm^2/V-s and the electron mobility is 6×10^{-3} cm^2/V-s which compares very well with the reported mobility values in literature for Pentacene ambipolar transistors.[3]

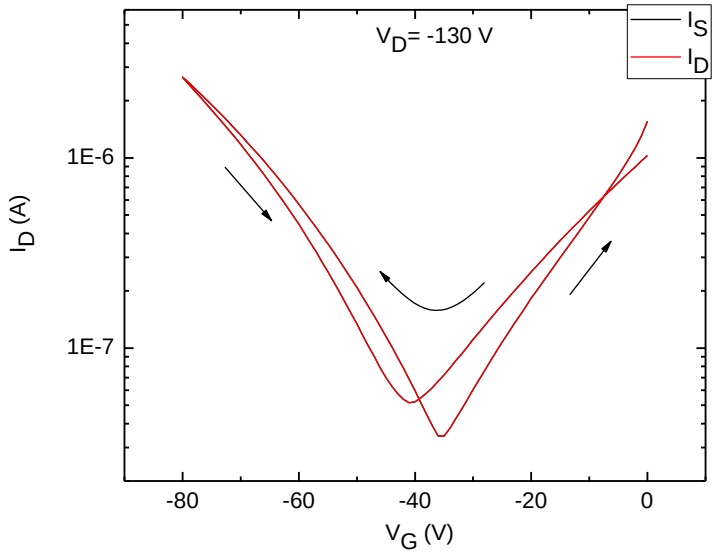

(a) Transfer characteristics of Pentacene ambipolar transistor at negative applied Drain voltage

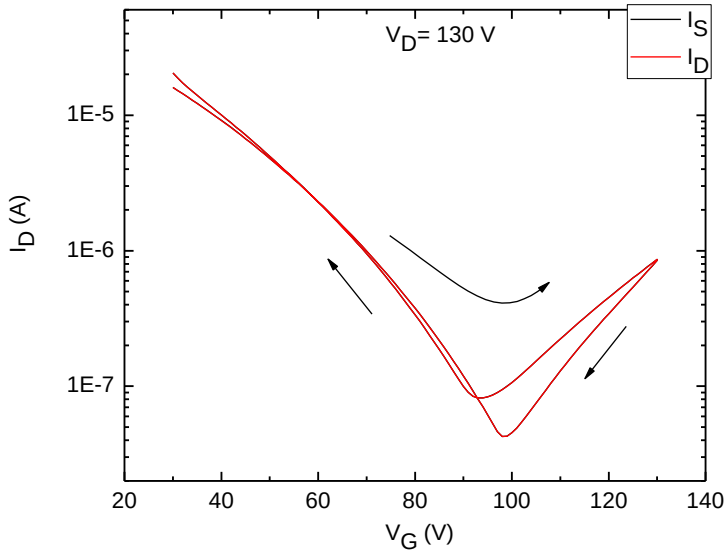

(b) Transfer characteristics of Pentacene ambipolar transistor at positive applied Drain voltage

Figure 23: Transfer curves of Pentacene transistors for positive and negative applied gate bias

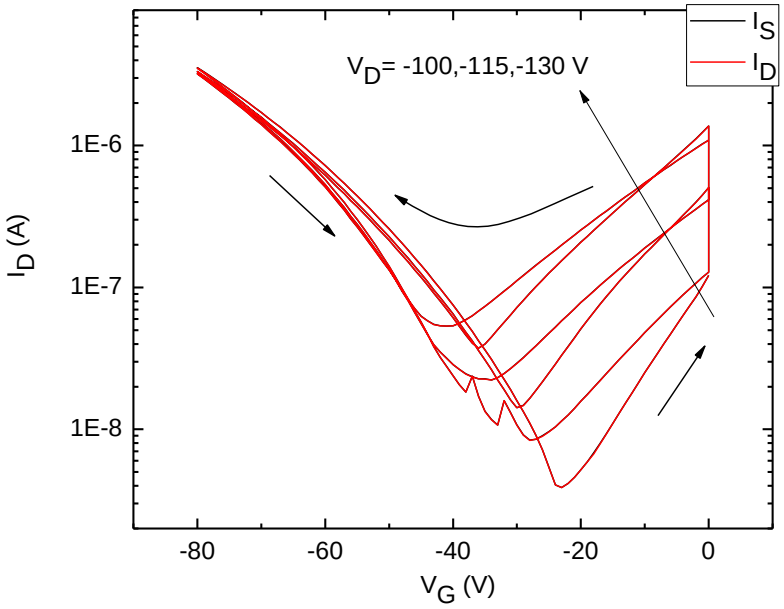

(a) Transfer characteristics of Pentacene ambipolar transistor at different negative applied Drain voltages

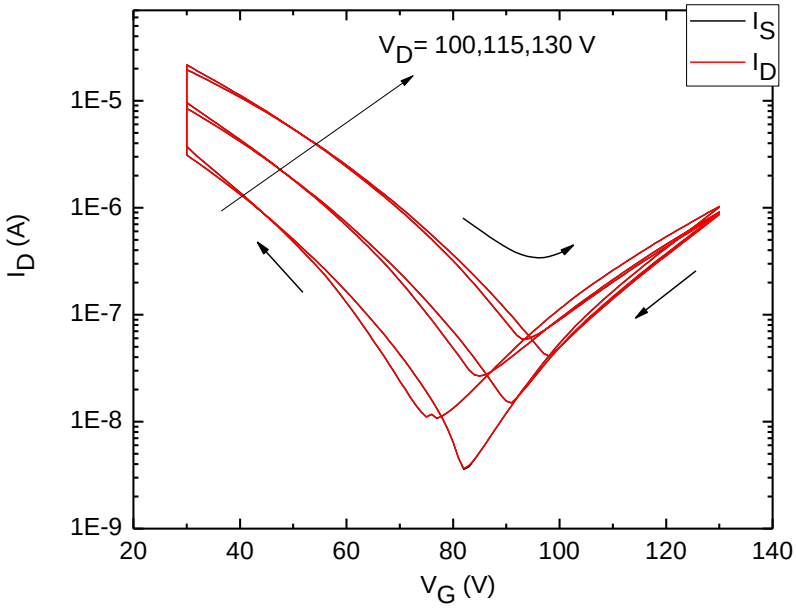

(b) Transfer characteristics of Pentacene ambipolar transistor at different positive applied Drain voltages

Figure 24: Transfer curves as a function of drain voltage for positive and negative applied gate bias

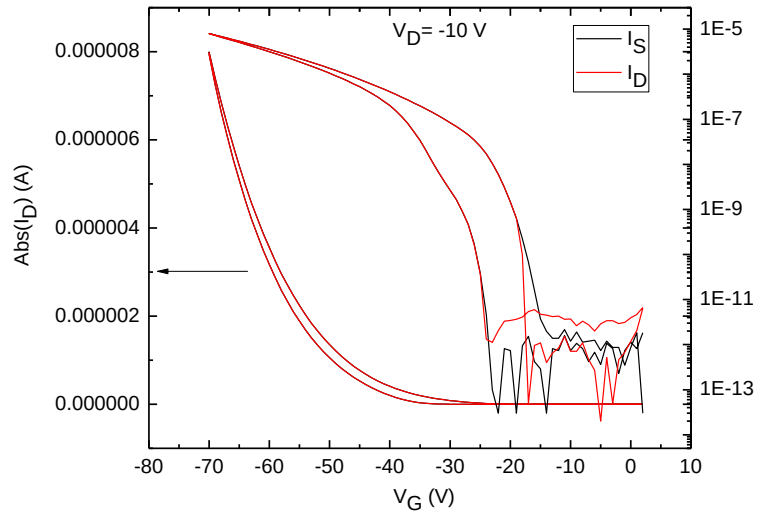

(a) Transfer curve at low applied negative Drain voltage (p-type)

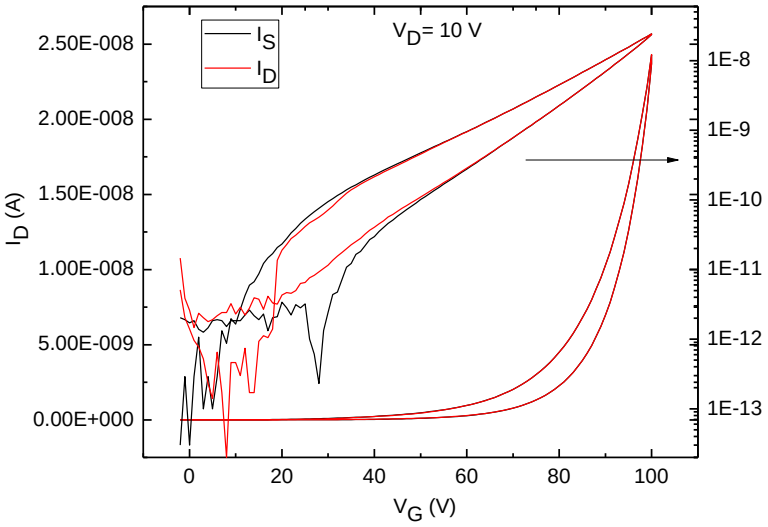

(b) Transfer curve at low applied positive Drain voltage (n-type)

Figure 25: p and n type transfer characteristics at low applied drain voltage for Pentacene transistors

4.4 Ambipolar BSBP transistors

BSBP transistors were fabricated following a similar procedure as reported.[5] However, these devices showed significant deviation from the reported values. The threshold voltage for both holes and electrons was much higher and as a result the ambipolar curves were obtained at much higher applied drain voltage. Fig. 26(a) shows the obtained ambipolar transfer characteristics at a applied drain voltage of -175V which is significantly higher then the reported values. To improve the charge injection, we put a thin Pentacene layer below Al source drain contact similar to a transistor architecture for ambipolar BP3T transistor reported by Yamane et.al.[7] This modification improved the current levels in ambipolar BSBP transistors as shown in fig. 26(b). However, the threshold voltage still remained higher than the reported values.[5]

Fig. 27 shows low drain voltage transfer characteristics of BSBP transistors. Hole and electron mobility of BSBP transistors is again calculated in a similar manner as Pentacene transistors. Hole mobility for BSBP devices is 9×10^{-4} cm^2/V-s and the electron mobility is 8×10^{-5} cm^2/V-s. These mobilities differ significantly from the reported values.[5]

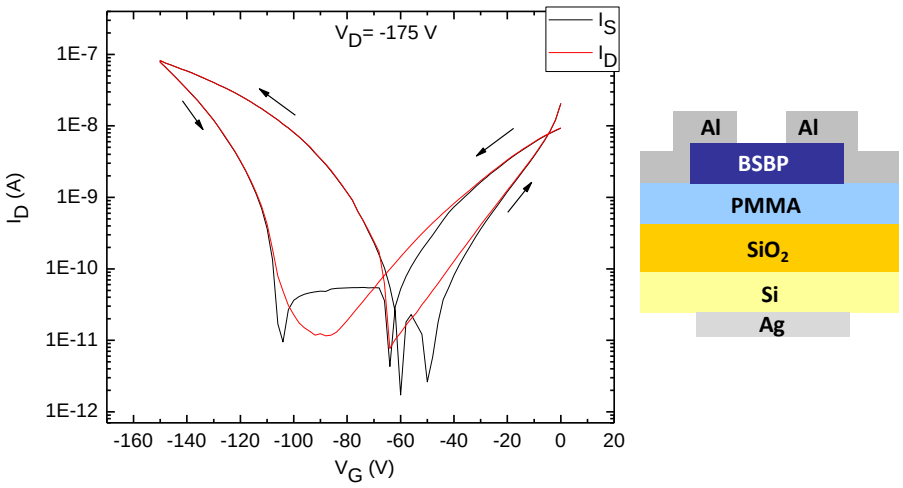

(a) BSBP transfer characteristics without Pentacene underlayer on S-D contacts

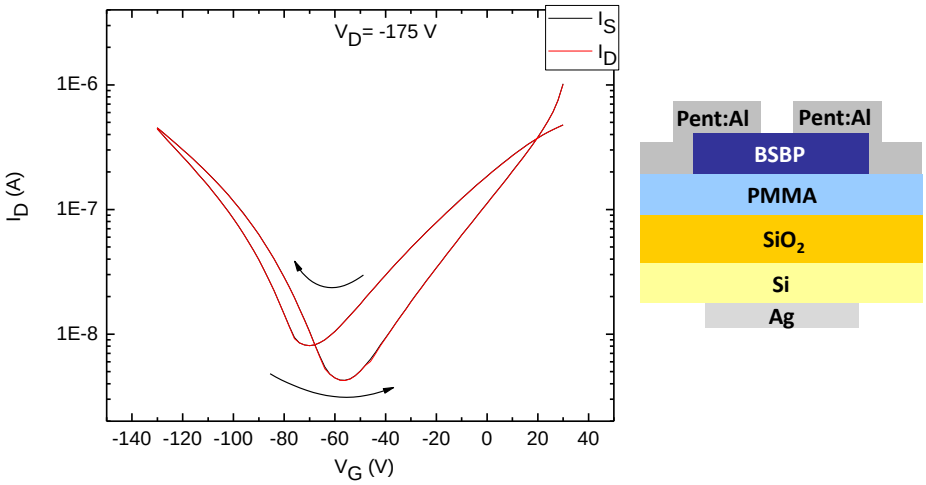

(b) BSBP transfer characteristics with Pentacene underlayer on S-D contacts

Figure 26: Transfer characteristics comparison of BSBP transistors with and without Pentacene under the contacts

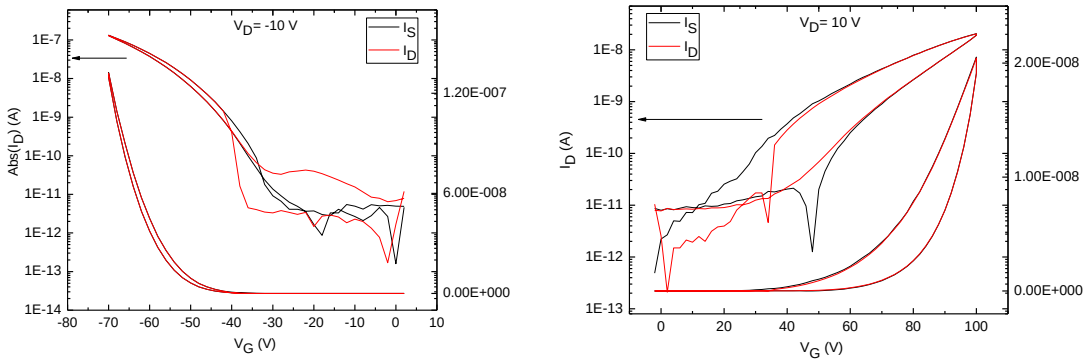

(a) Transfer characteristics for negative applied Gate voltage(p-type)

(b) Transfer characteristics for positive applied Gate voltage(n-type)

Figure 27: p and n type transfer characteristics at low applied drain voltage for BSBP transistors

In order to understand the origin of higher observed threshold voltage we carried out AFM measurements on BSBP and PMMA films. AFM images of thin film of BSBP shows a crystalline film as shown in fig. 29. It has been previously reported that the roughness of semiconductor-dielectric layer affects the threshold voltage and transistor mobilities.[8]. Threshold voltage goes up with increasing dielectric film roughness while the mobility goes down with increasing roughness. AFM on underlying PMMA film shows a neat PMMA with rms roughness of 3 nm which is quite low. Low roughness of PMMA films suggest that the dielectric interface is not the primary reason for observed high threshold voltage and lower mobilities. Purity of the material is another critical parameter which affects the threshold voltage of organic transistors and might be the reason for observed deviations.[5]

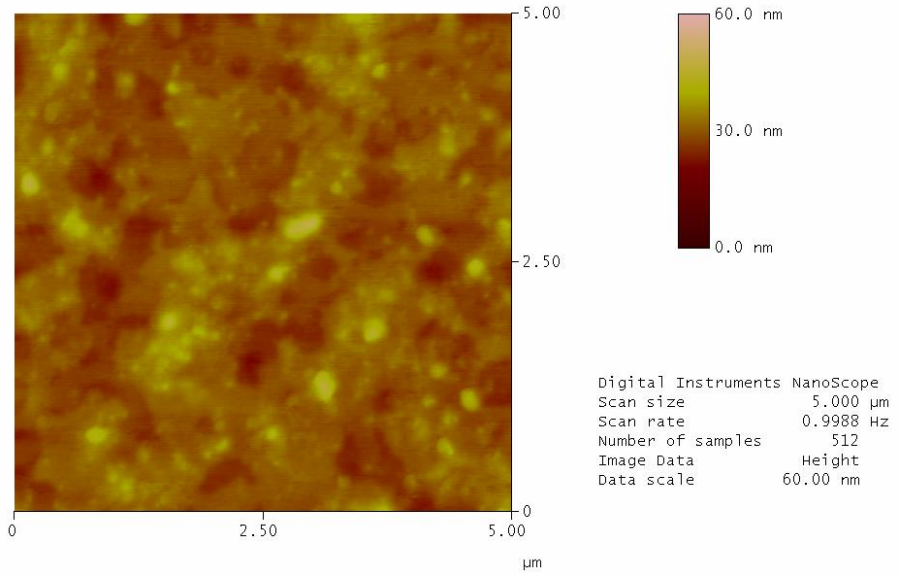

Figure 28: Tapping mode height AFM image of PMMA film

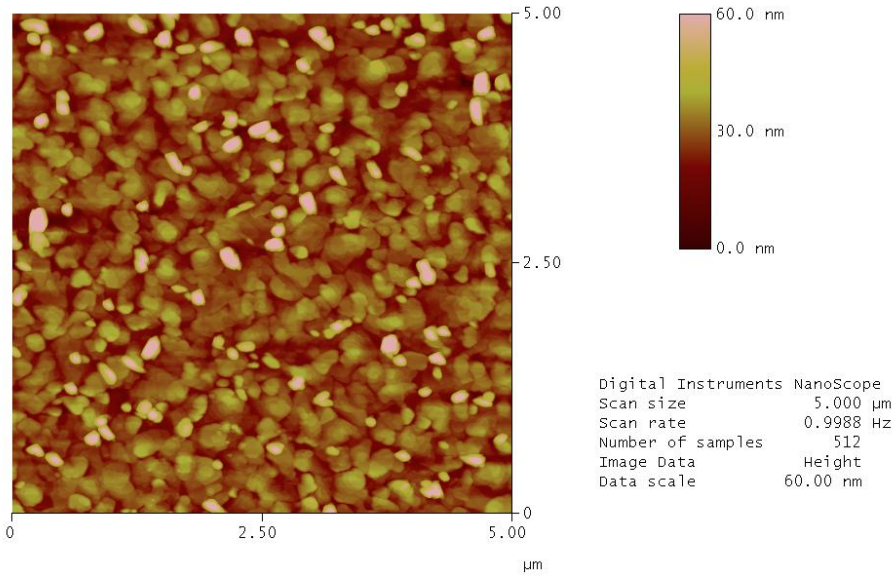

Figure 29: Tapping mode height AFM image of BSBP film

4.5 Pentacene tri-layer transistors

Recently, a vertical type of architecture was developed and reported which yields to improved device efficiency of OLETs.[4] These devices consist of an emissive layer is sandwiched between hole and electron transport layers. Holes are injected into the emissive layer through the p-type semiconductor and electrons and injected through n-type semiconductor. The HOMO and LUMO levels are aligned in such a way that the transfer of holes and electrons into the middle emissive layer is energetically favorable.[4] This sort of mechanism is more closer to the working principle of OLED rather than a transistor prompting us to study the exact working mechanism of such tri-layer type transistor architecture. It is desirable to understand the function of each individual layer in order to fully understand the working principle of tri-layer transistors. We modified the device architecture to include a Tetraphenylporphin(TPP) layer sandwiched between two Pentacene layers which carries both holes and electrons with Aluminum contacts. We fabricated several devices by excluding some of the individual layers and compared them with the tri-layer control device. This helped us to understand function of each layer separately. The device structure of the control device is shown in Fig. 30 along with the energy level diagram which helps us to understand the charge injection. For tri-layer devices, PMMA spin coated on SiO_2 substrates similar to Pentacene and BSBP transistors were used. A 300 $\mathring{A}$ layer of TPP was sandwiched between two 100 $\mathring{A}$ layers of Pentacene . 1000 $\mathring{A}$ Aluminum were used as top contacts. The channel length and widths were 100 μm and 3 μm respectively.

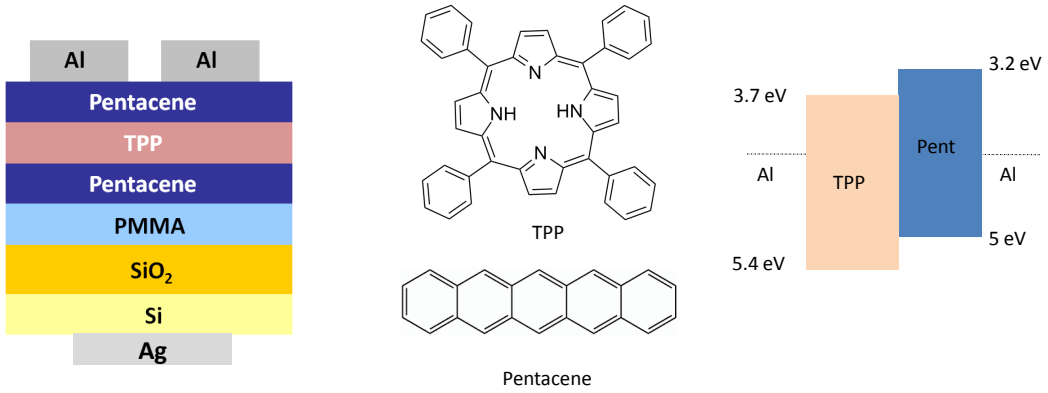

(a) Tri-layer control device with Pentacene and TPP

(b) Energy level diagram showing alignment of HOMO and LUMO levels with respect to contact work function

Figure 30: Device geometry of Pentacene-TPP tri-layer transistors along with the energy level diagram

Devices lacking the top Pentacene layer still showed ambipolar behavior as shown in fig. 31. However the hole current suppressed by an order of magnitude. This can be understood by considering the the energy level diagram of the two materials with Aluminum work function. The energy offset between HOMO level of Pentacene and Al is lower than energy offset between HOMO level of TPP and Al. This suggests that the hole injection from Al contacts into TPP is frustrated, reducing the hole current in TPP-Pentacene device as compared to the tri-layer control device.

However, devices lacking the bottom Pentacene layer displayed no hole transport and only n-type behavior was observed, as seen in in fig. 32. Pentacene-TPP device behavior was identical to the transfer characteristics of a neat TPP transistor as shown in fig. 33. This suggests that the charge transport is clearly confined to the semiconductor layer adjacent to the dielectric as one would expect intuitively. Clearly the top Pentacene layer in contact with the source-drain electrodes only serves to improve charge injection in the device because of its favorable alignment with work function of Al as compared to TPP. To determine if the

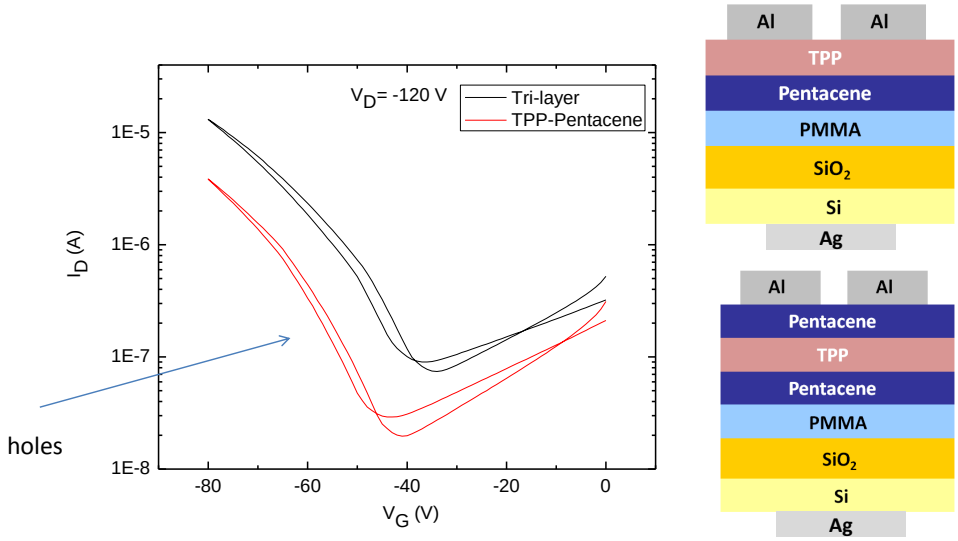

Figure 31: Transfer curve comparison of Tri-layer device with TPP-Pentacene device along with the device architectures

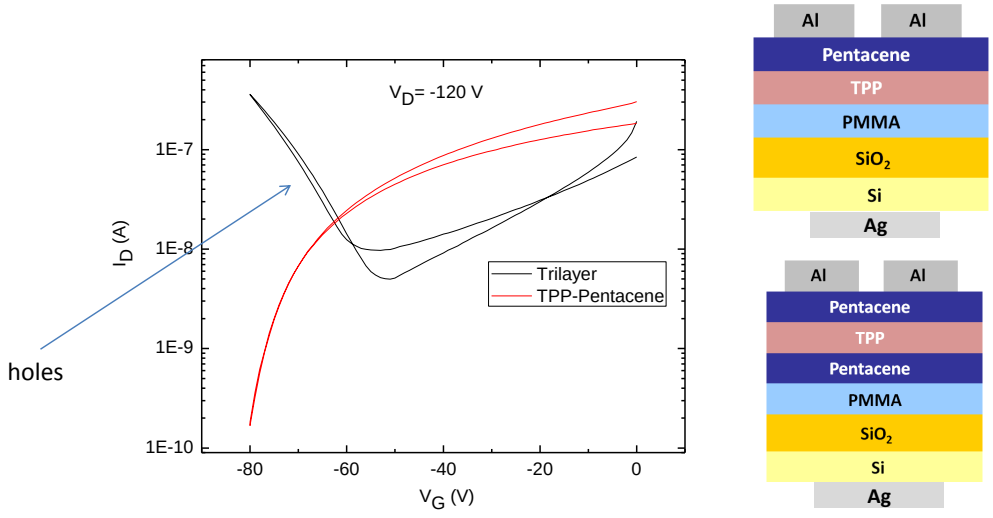

Figure 32: Transfer curve comparison of Tri-layer device with Pent-TPP device along with the device architectures

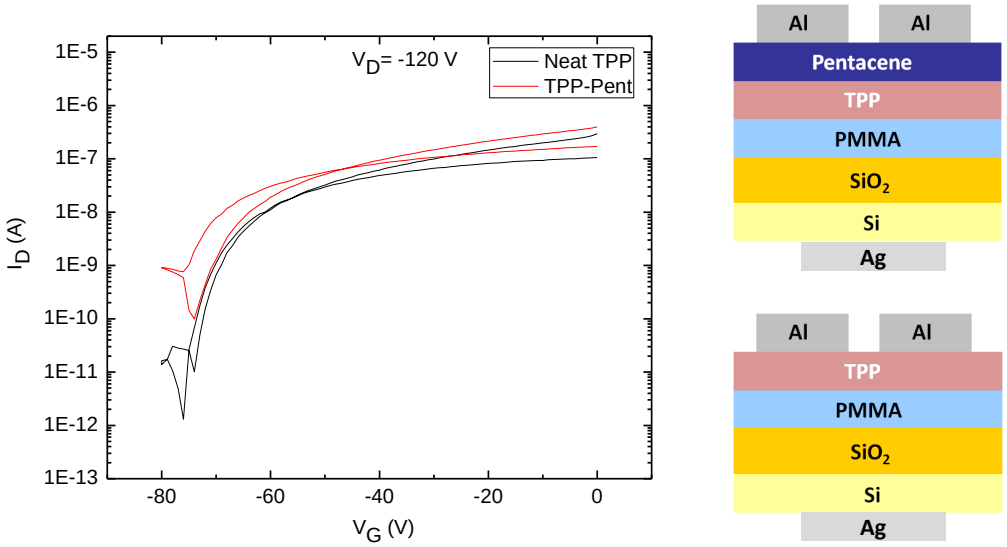

Figure 33: Transfer curve comparison of neat TPP device with Pent-TPP device along with the device architectures

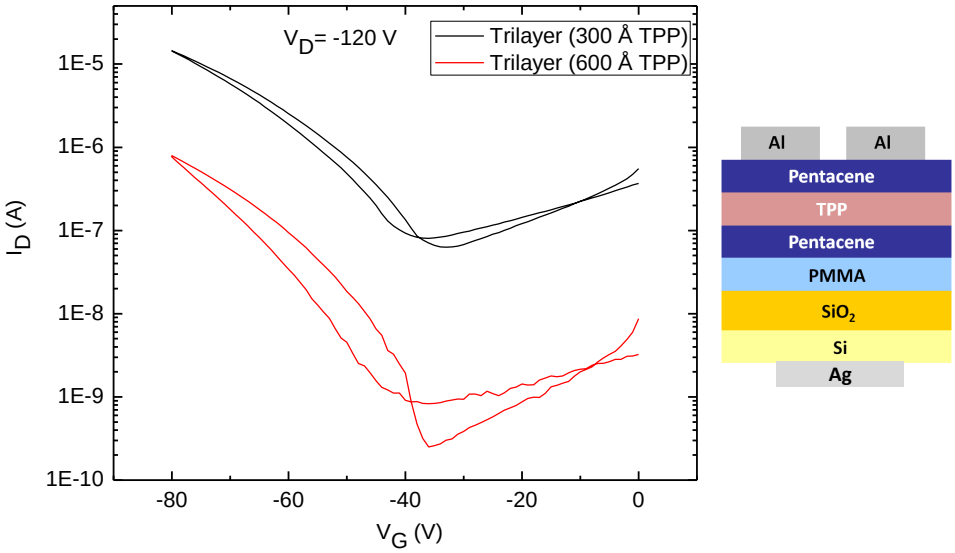

Figure 34: Transfer curve comparison of thick TPP device with control device

middle layer actually carries charge, we fabricated another device with 600 $\mathring{A}$ intermediate TPP layer and compared with the 300 $\mathring{A}$ intermediate TPP layer control device. The comparison is shown in fig.34 and clearly shows the current reduction at high TPP thickness. It is thus clear that charge transport is confined to the bottom layer and the top layers serve as injection layers. High thickness of TPP only increases the overall device resistance and thus reduces the current.

4.6 Conclusion

We successfully demonstrated ambipolar Pentacene transistors with symmetric Al contacts. The mobilities calculated compare well with the reported values. We also fabricated BSBP ambipolar transistors with symmetric Al contacts. However,these devices show significant deviation from the reported behavior. We attribute this deviation to purity of used BSBP material based on AFM images and roughness values of dielectric interface.

We also fabricated tri-layer transistors using Pentacene and TPP in order to get more insights on working of tri-layer transistors. We found out that the transistor charge transport is confined to the bottom-most layer and the top layers only aid the injection of charges into bottom layer. Thicker layers increase the resistance and reduces the drain current. Also, based on the alignment of work function of metal electrode with the energy levels of top layer, we expect more efficient charge injection in the case of better work function alignment.

References

[1] K. N. N. Unni, A. K. Pandey, S. Alem and J.-M. Nunzi, Chem. Phys. Lett. **421**, 554 (2006).

[2] R. Capelli, F. Dinelli, M. A. Loi, M. Murgia, R. Zamboni and M. Muccini, J. Phys.: Condens. Matter **18**, S2127 (2006).

[3] C. Yang, S. Cheng, C. Ou, Y. Chuang, M. Wu and C. Chu, J. Appl. Phys. **103**, 094519 (2008).

[4] R. Capelli, S. Toffanin, G. Generali, H. Usta and A. F. . M. Muccini, Nature Materials **9**, 596 (2010).

[5] T. Sakanoue, M. Yahiro, C. Adachi, H. Uchiuzou, T. Takahashi and A. Toshimita, Appl. Phys. Lett. **90**, 171118 (2007).

[6] J. S. Swensen, J. Yuen, D. Gargas, S. K. Buratto and A. Heeger, J. Appl. Phys. **102**, 013103 (2007).

[7] K. Yamane, H. Yanagi, A. Sawamato and S. Hotta, Appl. Phys. Lett. **90**, 162108 (2007).

[8] S. E. Fritz, T. W. Kelley and C. D. Frisbie, The Journal of Physical Chemistry B **109**, 10574 (2005), [http://pubs.acs.org/doi/pdf/10.1021/jp044318f], PMID: 16852282.

[9] M. Schidleja, C. Melzer and H. von Seggern, Appl. Phys. Lett. **94**, 123307 (2009).

[10] Y. Liang, C. D. Frisbie, H.-C. Chang and P. P. Ruden, Jour. Appl. Phys. **105**, 024514 (2009).

[11] L. Yan, *Examination of transient carrier behaviors in organic field-effect devices via displacement current measurement*, PhD thesis, University of Minnesota, Jan 2011.

[12] M. Schidleja, C. Melzer and heinz von Seggern, Frequenz **62**, 100 (2008).

[13] D. L. Smith and P. P. Ruden, Appl. Phys. Lett. **89**, 233519 (2006).

5 Study of F8BT transistors

5.1 *Introduction*

Since the advent of ambipolar organic light emitting transistors (OLETs), research is mainly focussed on developing materials and devices that exhibit ambipolar behavior and also have good light emitting properties. However, there are only a few materials that have both good transistor properties and also emit light. One of the materials that has been studied extensively is a green light emitting polymer Poly(9,9-di-n-octyl-fluorene-alt-benzothiadiazole) (F8BT).[1] F8BT works as a light emitting transistor in top gate,bottom contact geometry. Research on F8BT is focused on improving its device performance by varying its morphology,using a high capacitance dielectric and also modifying the contacts with SAM layers to improve charge injection.[2] [3] [4] [5] However, as discussed before, it is desirable to separate the functions of charge transport and light emission on two different molecules. This can be achieved by using a dopant in small amount to which the excitons from F8BT can be energy transferred. In order to investigate energy transfer, we used a red-emitting molecule Tetraphenylporphyrin (TPP) as a dopant. We fabricated light emitting transistors using F8BT by following the procedure reported in literature [1] and modified the structure to a bi-layer F8BT-TPP geometry. We report the results obtained by varying the TPP thickness, baking temperature of the TPP layer in this chapter along with rough calculation of External Quantum Efficiency(EQE) and photocurrent measurements.

5.2 *Experimental Details*

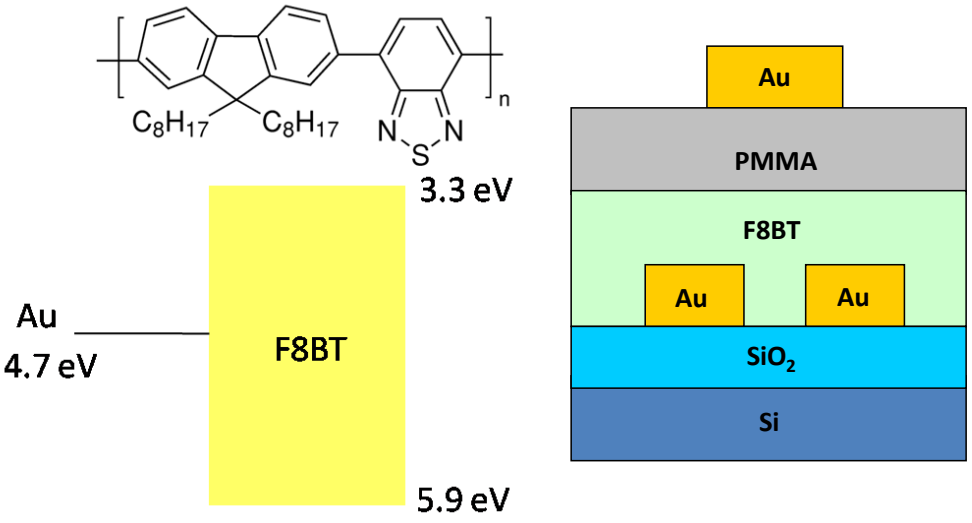

Figure 35: Energy bands and structure of fabricated F8BT devices

F8BT transistors were fabricated by following the experimental technique as described in literature.[1] Bottom inter-digitated source-drain electrodes were photolithographically patterned followed by Au evaporation in clean room. The channel length of the pattern was 30 μm and the channel width was 5000 μm. The devices had 10 interdigitated fingers patterned. A 20mg/ml solution of F8BT(M_w ≈15,000) in anhydrous Toluene was stirred overnight at 65°C. F8BT films were spin coated inside the glove-box at 2000 RPM for 1 min. This speed was chosen such that the obtained film thickness was in a range of 600-800 $\mathring{A}$. Samples were baked at 290°C for 15 minutes and then quenched on a metal plate. Approximately 40 mg/ml solution of PMMA(M_w ≈120,000) in anhydrous n-butyl acetate was stirred overnight at 110°C. Spin speed for PMMA was chosen to be 2800 rpm in order to obtain film thickness of about ≈ 3000 $\mathring{A}$. The device was again baked at 120°C to get rid of the solvents completely. In the experiments involving TPP, various thicknesses of TPP were thermally evaporated over F8BT before spinning PMMA on the top. Semi-transparent,120

$\mathring{A}$ of Au was evaporated on the top through a patterned shadow masks to complete the device. All the processing was carried out inside a Nitrogen glovebox in order to avoid air exposure. The devices were then transferred to probe station glovebox and tested. Optical spectra were obtained with 1000 μm optical fibre and Ocean optics HR4000 spectrometer. Newport 818-ST photodetector was used to carry out photocurrent measurements. Both the photodetector and spectrometer fiber were aligned over the top of the light emitting device in order to collect light. The device geometry and energy band picture is shown in fig.35. As seen from the energy band picture work function of Au lies in the middle of the F8BT band gap and thus allows efficient hole and electron injection in bottom contact-top gate geometry.[1]

5.3 Ambipolar F8BT transistors

F8BT transistors were tested in a inert atmosphere glove-box without air exposure. Measured transfer curves and calculated mobility values are comparable with reported values. Figure 36 shows the transfer curves obtained on one of the device for both positive and negative applied drain voltage. The curves show very symmetric V-shaped transfer curves with low electron and hole threshold voltage. Linear hole and electron mobilities were calculated from this data. The devices showed hole mobility of $\mu_{holes} = 2 \times 10^4$ cm^2/V-s and electron mobility of $\mu_{electrons} = 3 \times 10^5$ cm^2/V-s which compares well with the reported mobility values.

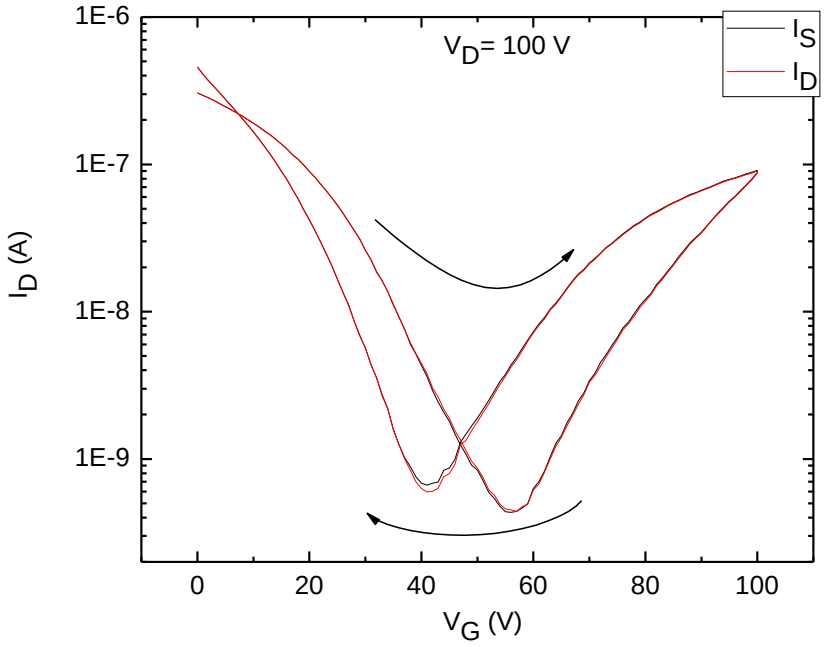

(a) Transfer characteristics of F8BT ambipolar transistor at positive applied Drain voltages

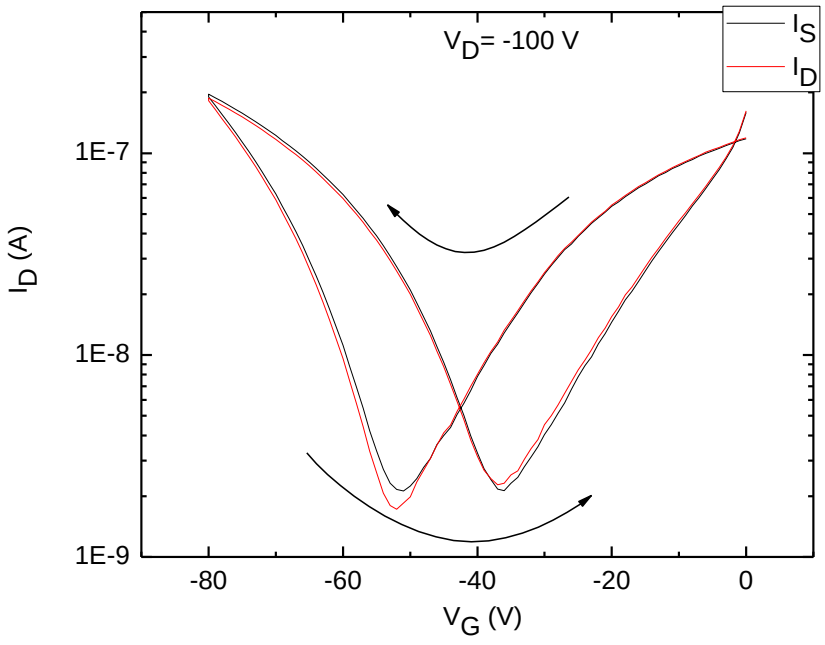

(b) Transfer characteristics of F8BT ambipolar transistor at negative applied Drain voltages

Figure 36: Ambipolar transfer curves of neat F8BT devices for positive and negative applied gate voltages

5.4 Study of F8BT-TPP system

As discussed before in previous chapters, although OLETs are interesting in terms of integrating properties of OLEDs and transistor switching into one device there are not many materials that have both ambipolar charge transport properties and will emit light efficiently. Taking cue from OLEDs, where host-guest type of structures are widely used, it will be interesting to employ the same concept in OLETs. Host molecule should have good ambipolar transistor properties while the guest molecule will ensure energy transfer of excitons from the host and efficient light emission. We looked at TPP as a potential candidate for the guest to be used with F8BT light emitting transistors.

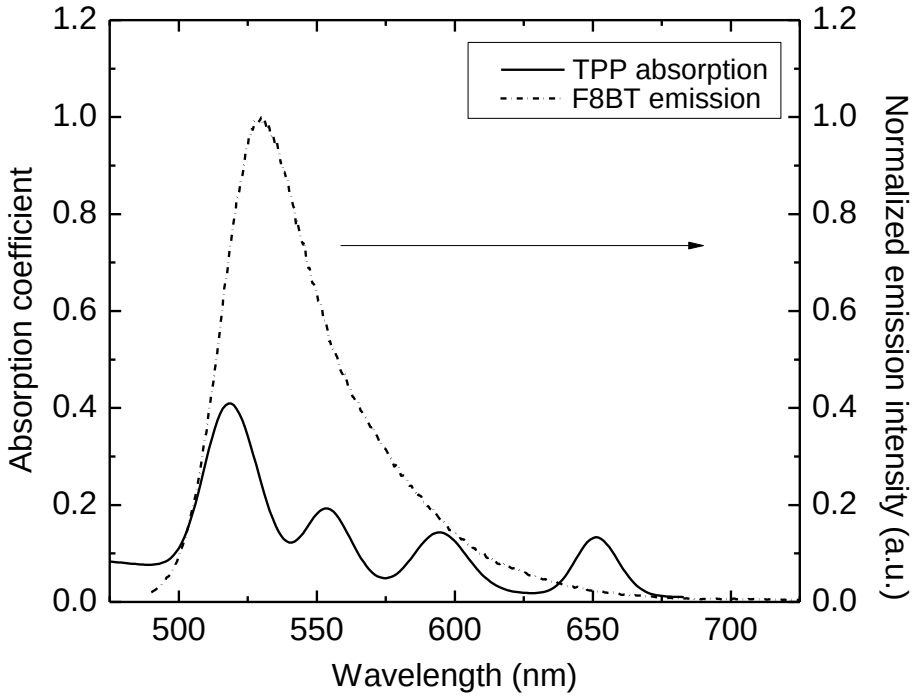

Figure 37: Overlay of F8BT(host) emission and TPP(guest) absorption

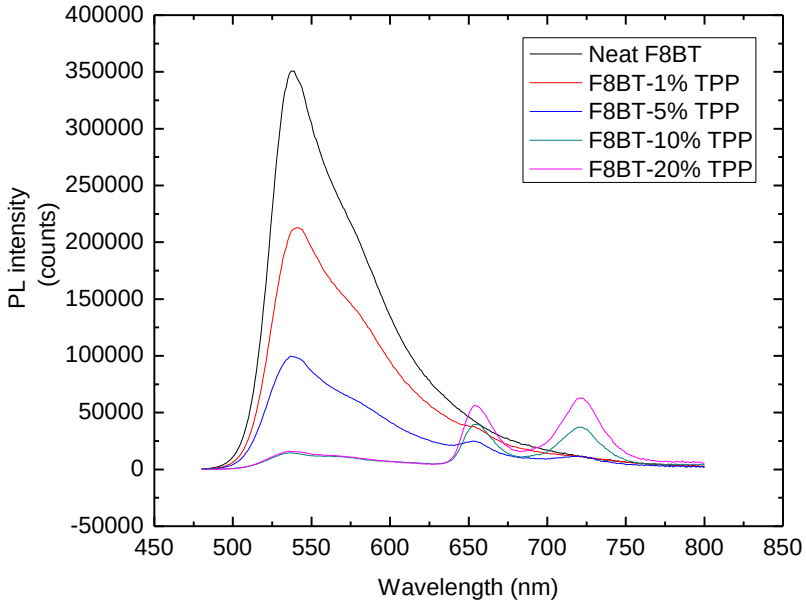

(a) PL emission spectra of F8BT-TPP films as a function of TPP concentration

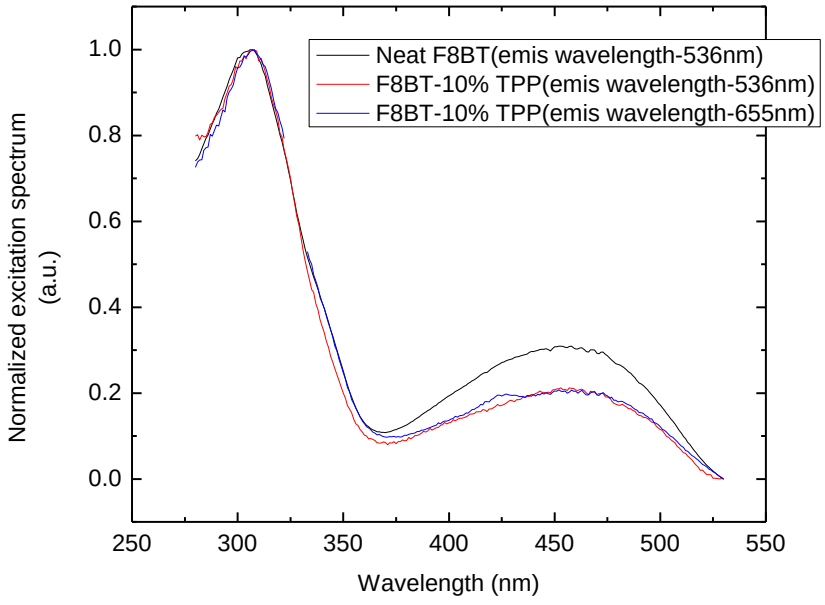

(b) Excitation spectra of F8BT-10%TPP film with emission wavelength fixed at 536nm and 655nm

Figure 38: PL measurements on F8BT-TPP films as a function of varying TPP concentration

In order to have energy transfer from host to guest, an overlap between the emission spectrum of the host molecule and absorption spectrum of the guest molecule is necessary. Fig.37 shows overlap of F8BT emission and TPP absorption suggesting possibility of energy transfer between two molecules. In order to investigate whether F8BT and TPP are compatible in terms of showing good energy transfer, we looked at the concentration dependence of TPP doped F8BT films by measuring photoluminescence(PL) spectra of F8BT-TPP films with varied dopant concentration. Fig.38(a) shows PL emission spectra of F8BT-TPP films as a function of TPP concentration. As seen clearly from the PL spectra, as TPP concentration is increased the F8BT peak emission (at 536nm) goes down and TPP emission peaks (at 655 nm and 720 nm) increase in intensity. Fig.38(b) shows excitation spectra obtained on F8BT-10%TPP film by fixing emission wavelength to 536 nm and 655 nm along with excitation spectrum of neat F8BT film at fixed emission wavelength of 536 nm on the same plot. Based on similar nature of the obtained excitation spectra it can be concluded that there is energy transfer between F8BT and TPP.

PL measurements on F8BT-TPP films were also carried out with spin coated PMMA as dielectric layer on the top. It was observed that spinning PMMA layer on top of F8BT-TPP films resulted in reduction of TPP emission intensity relatively in comparison with F8BT peak as depicted in fig.39. This causes F8BT peak to dominate in the spectrum which is undesirable while measuring electroluminescence(EL) spectra. This problem can be attributed to the solubility of TPP in n-butyl acetate which is used as solvent for PMMA. This prompted us to modify the device geometry into a bi-layer type of structure with neat layers of F8BT and TPP. The idea is to have enough TPP over the top of F8BT such that it does not get completely washed out as PMMA is spin coated on the top. Further baking after the PMMA spin coating step will allow F8BT and TPP to intermix possibly leading to energy transfer between the two molecules.

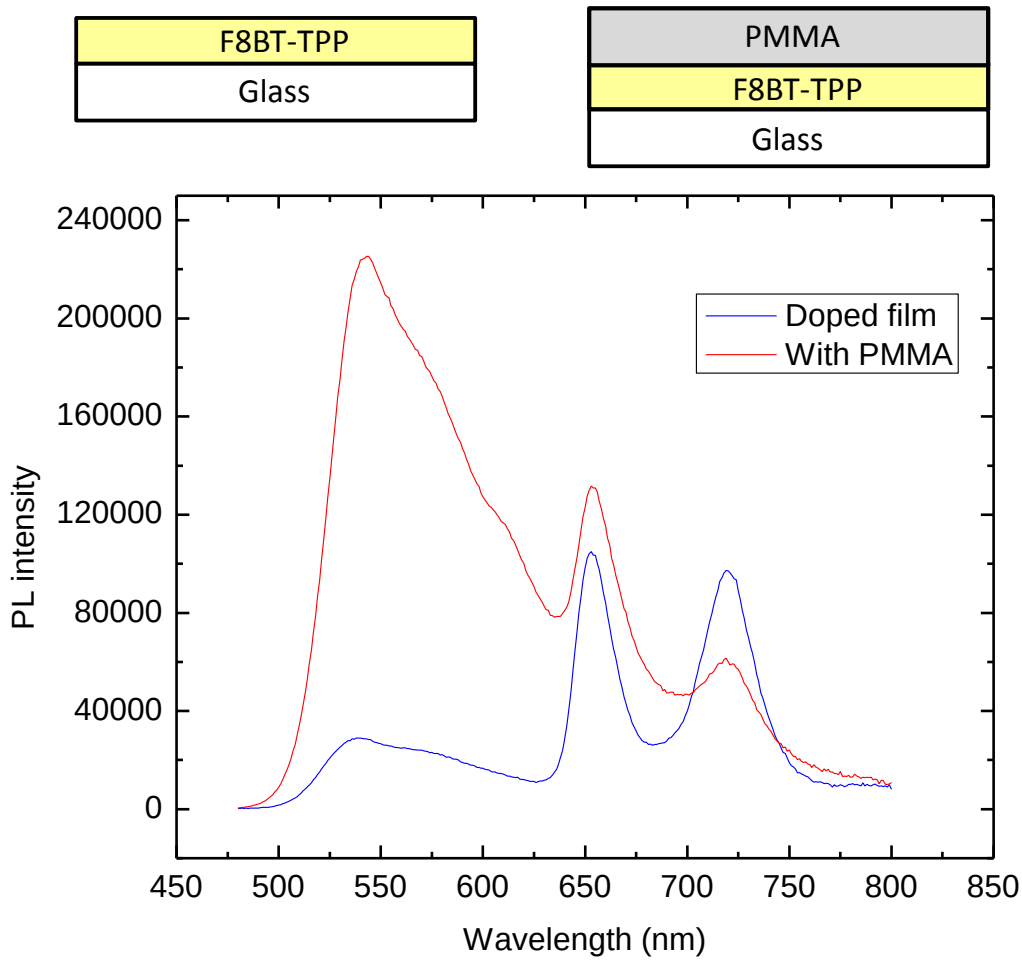

Figure 39: PL spectrum of F8BT-TPP film showing effect of PMMA spin coating on F8BT peak

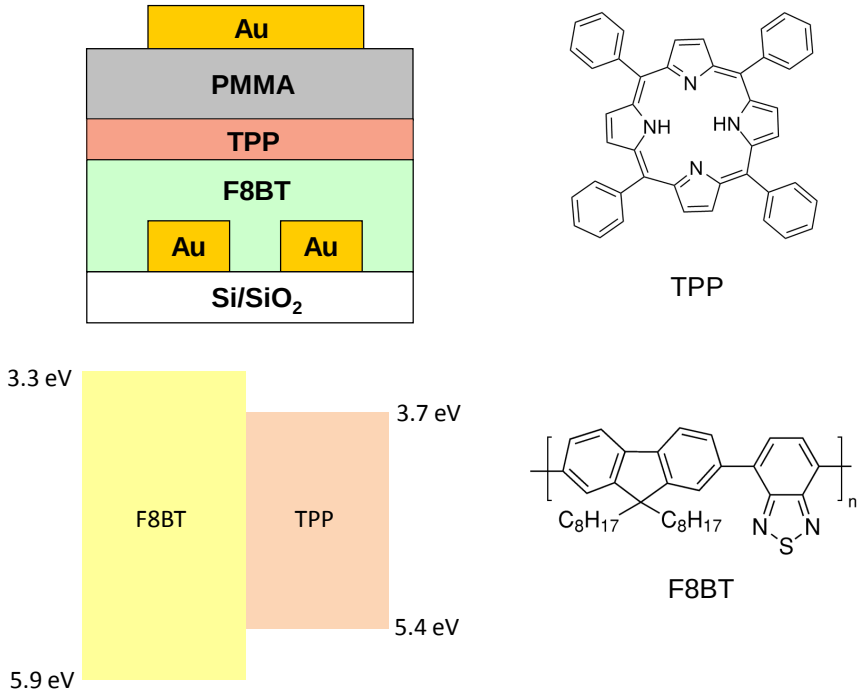

Figure 40: Device structure for F8BT-TPP bi-layer transistors

5.5 F8BT-TPP bi-layer devices

As seen from the previous discussion, spin coating PMMA on top of F8BT-TPP mixed film has undesirable consequences in terms relative emission of F8BT and TPP. As a result, we switched to F8BT-TPP bi-layer system. The devices were tested electrically and optically as a function of TPP thickness and also as a function of baking time of the devices. F8BT-TPP bi-layer devices were fabricated with varying thickness of the top TPP layer. Fig.40 shows the schematic of F8BT-TPP bilayer devices and corresponding energy band diagram. TPP thickness was varied in between 50$\mathring{A}$ to 200$\mathring{A}$.

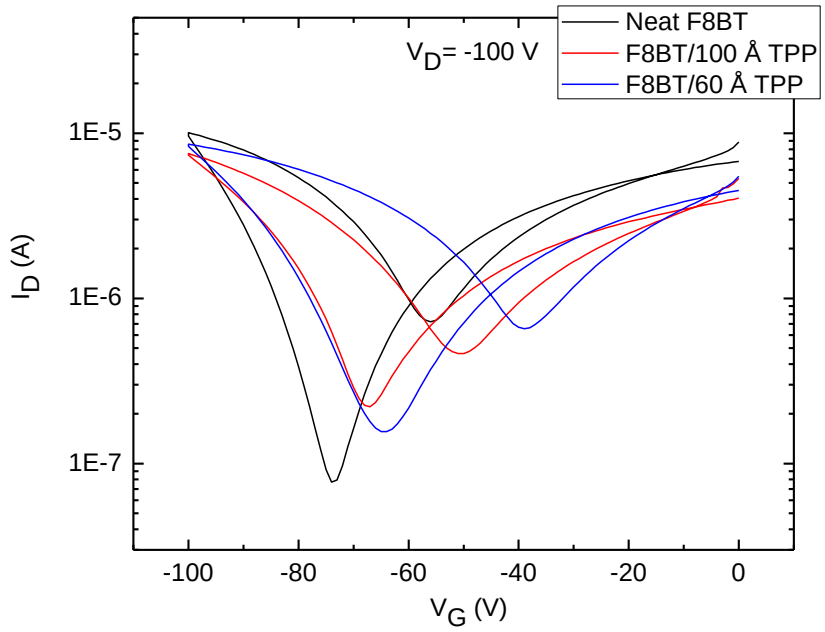

Figure 41: Transfer curve comparison for neat F8BT and F8BT-TPP bilayer devices

5.5.1 TPP thickness dependence

Fig.41 shows comparison of transfer curves for neat F8BT and bi-layer devices. Both hole and electron current decreases slightly at higher TPP thickness as expected due to extra device resistance. However, the current at the V-shaped neck point (the region where holes and electrons co-exist in the channel and lead to light emission) still remains comparable. This suggests that the number of excitons does not change significantly with added TPP layers. Also, based on the fact that the shape and magnitudes of transfer curves is very similar to each other, we can argue that F8BT layer is still carrying holes and electrons from source to drain and charge transport if not hampered by addition of TPP layers. In addition to similar transfer characteristics, both hole and electron mobilities calculated from the transfer curves are comparable in bi-layer devices providing further evidence of charge transport in F8BT. Calculated hole and electron mobilities in neat F8BT control device are 1.2×10^4 cm^2/V-s and 2.7×10^5 cm^2/V-s respectively. Whereas, hole and electron mobilities for F8BT-100$\mathring{A}$ TPP device are 1×10^4 cm^2/V-s and 2.3×10^5 cm^2/V-s respectively.

To obtain the electroluminescence(EL) spectrum of the devices, the device was run at fixed applied voltage. The drain voltage was kept constant at -100V while the gate voltage was kept at -75V. Photocurrent measurements on these devices show a maximum photocurrent output at this biasing condition, prompting the use of these biasing voltages while collecting the EL spectra. The integration time was 20 sec.and the data points were averaged 5 times before recording the spectra. Fig.42 shows the comparison of EL spectrum for two different TPP thicknesses in comparison to F8BT control device. In order to compare the relative magnitudes of F8BT and TPP peaks the spectra were normalized with respect to the maximum intensity obtained at F8BT emission peak. Emission peak of F8BT is observed around 540nm while TPP emits at 655nm and 720nm. As seen from the spectra, as the TPP thickness goes up the emission peaks from TPP increase in magnitude relatively

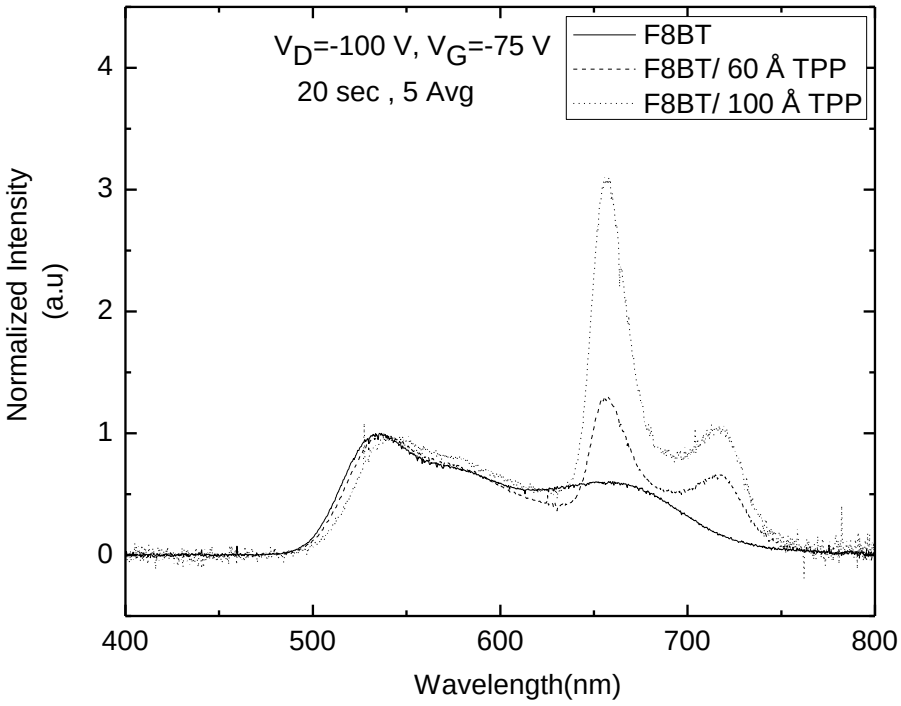

Figure 42: Electroluminescence spectra obtained for neat F8BT and bilayer devices as a function of TPP thickness

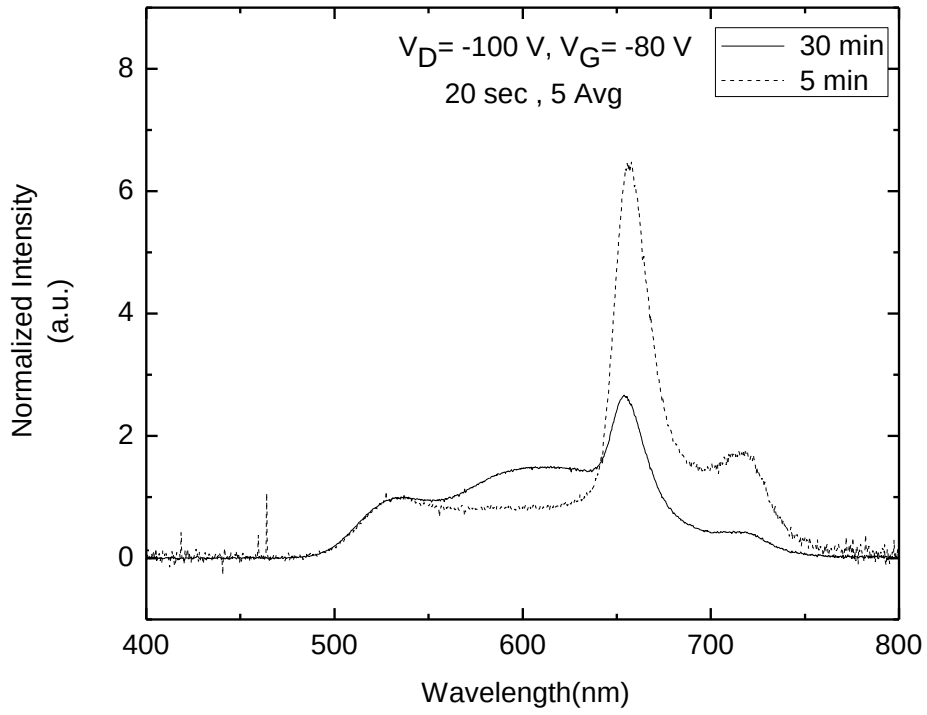

Figure 43: Electroluminescence spectra obtained for neat F8BT and bilayer devices at two different baking times

in comparison with F8BT emission. This can be attributed either to energy transfer between F8BT and TPP or just the absorption and re-emission in TPP layer without energy transfer.

5.5.2 Baking time dependence

In order to improve emission from TPP molecules we changed the baking time after spinning PMMA film and compared the spectra. The idea was to have as much intermixing of F8BT and TPP possible due to baking. Spectra obtained from the devices at two different baking times are shown in fig.43. The results obtained are counter-intuitive. As seen from the

figure the lower baking time gives more relative emission intensity from TPP suggesting that the idea of intermixing the two layers is not valid. However, it is difficult to to probe the F8BT-TPP interface in order to have better understanding of the emission mechanism in bi-layer devices.

5.5.3 AFM study of F8BT-TPP devices

To co-relate obtained emission spectra with morphology in bi-layer devices, we carried out AFM measurements on the devices at different stages of device fabrication. Both neat F8BT and F8BT-80$\mathring{A}$ TPP samples were made following same process as device fabrication. Some samples were treated with anhydrous n-butyl acetate(solvent of PMMA) in order to stud effect of solvent on films. AFM images were taken inside channel region.Figure 44(a) shows the F8BT-80$\mathring{A}$ TPP film without solvent treatment and it can be seen that evaporated TPP forms a uniform film on top of spin coated F8BT. However, when treated with the solvent the film morphology changes drastically and looks like domains of polymer chains intermixed together as seen in fig.44(b). Neat F8BT AFM image shows clear domains as shown in fig.45(a). It has been reported that, F8BT forms crystalline film when annealed at 290°C.[5] However neat F8BT film treated with solvent again shows similar intermixed structure as seen in fig.45(b). In both cases, phase image tracks the height image profile making it difficult to distinguish between the phases based on AFM imaging. From these measurements it is hard to conclude anything about the film morphology in the actual device and hence as a result it becomes tough to predict the exact emission mechanism in these bi-layer devices.

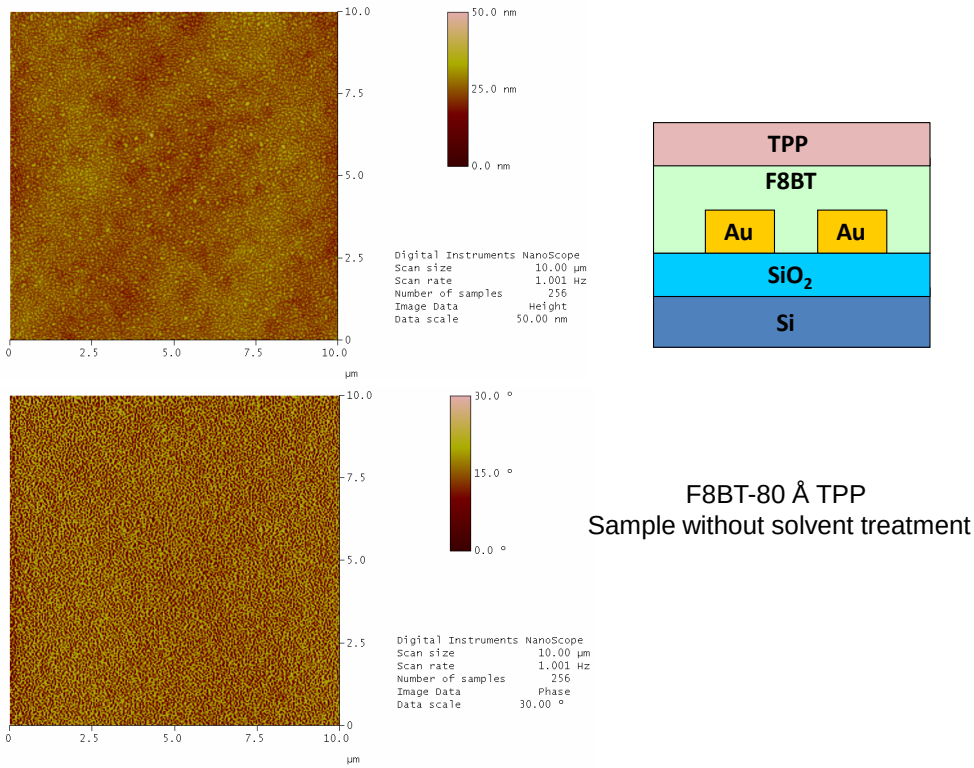

(a) Tapping mode AFM image of F8BT-80 $\mathring{A}$ TPP film without solvent treatment

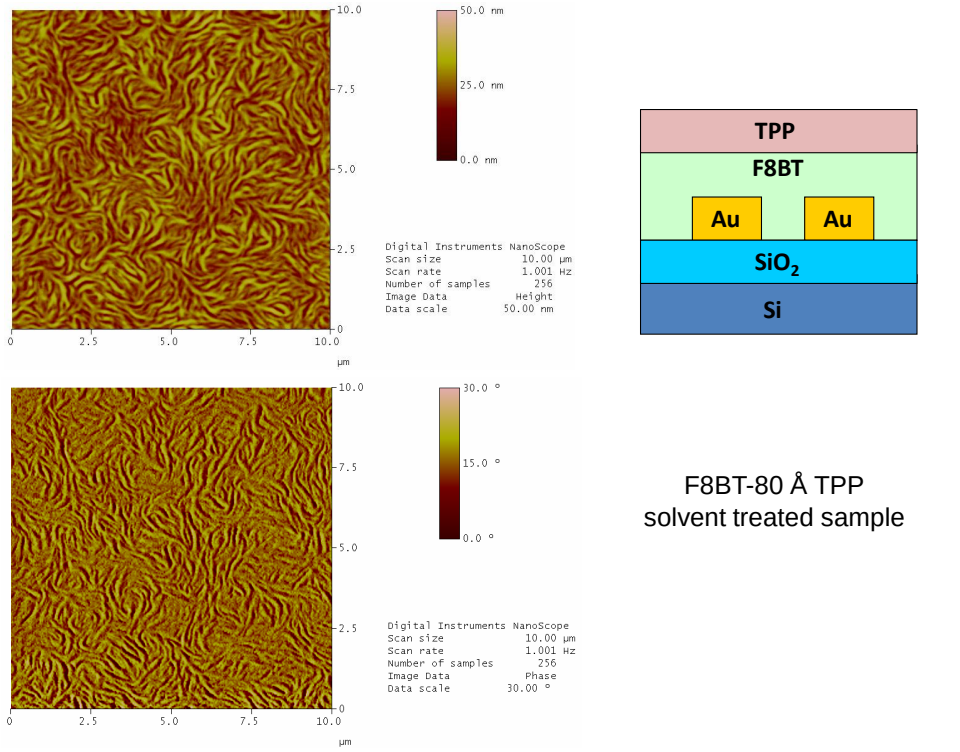

(b) Tapping mode AFM image of F8BT-80 $\mathring{A}$ TPP film with solvent treatment

Figure 44: AFM images of F8BT-TPP films with and without solvent treatment

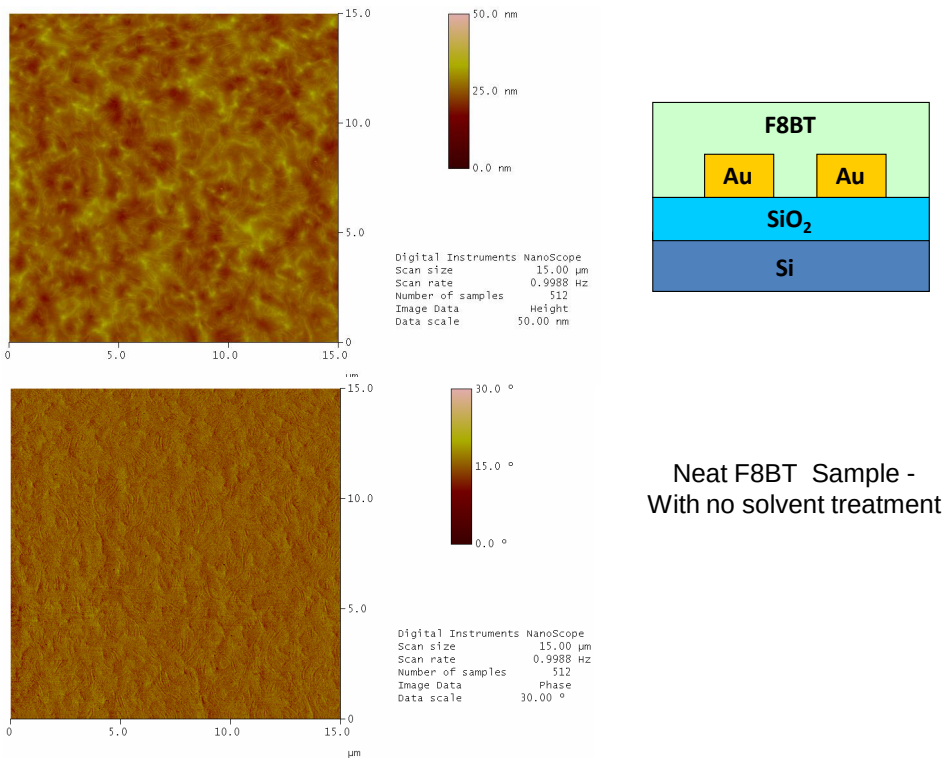

(a) Tapping mode AFM image on neat F8BT sample without solvent treatment

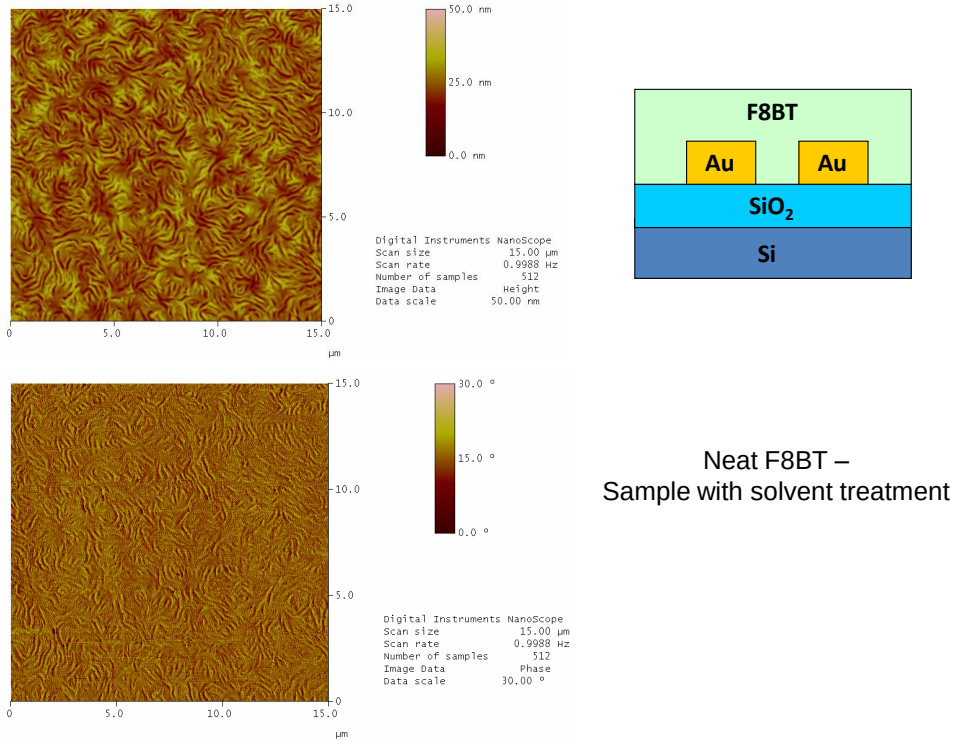

(b) Tapping mode AFM image on neat F8BT sample with solvent treatment

Figure 45: AFM images of neat F8BT-TPP films with and without solvent treatment

5.6 Photocurrent measurements and EQE calculations

Photocurrent measurements were carried out as a function of gate voltage at a constant drain voltage. As the gate voltage is swept the emission zone moves inside the channel and the amount of light emitted also changes.[1][6] Amount of light emitted can be thought to be dependent on number of electrons and holes present into the channel and thus can be related to the measured drain current. It is also important to note that light emission will be observed only when both holes and electrons are present in the channel. So we should expect no light output at the extremes of the voltage sweep where the transistor is operating in unipolar mode.

5.6.1 Photocurrent measurements

Photocurrent measurements on various F8BT-TPP bi-layer devices were performed with the photodiode lying on the top of the device while the gate voltage is swept. Since not all the light emitted is collected this way this method tends to underestimate the photocurrent and thus in turn the EQE of these devices. The values obtained are thus quite low as compared to reported values. However, the trends obtained during these measurements are still worth noting.

Fig.46 shows the photocurrent data collected during voltage sweeps on devices with different TPP thickness. While photocurrent measurement data for the baking time variation is shown in fig.47. As seen from the data, two clear peaks are observed in the photocurrent measurements on either side of ambipolar region of measured transfer curve. The peaks can be thought of an interplay between the transition between unipolar emission from one side to ambipolar emission in the middle and also due to the decrease in number of electrons and holes in the channel in ambipolar region. Ambipolar light emission will be more efficient than unipolar emission and this is confirmed from calculated EQE values.

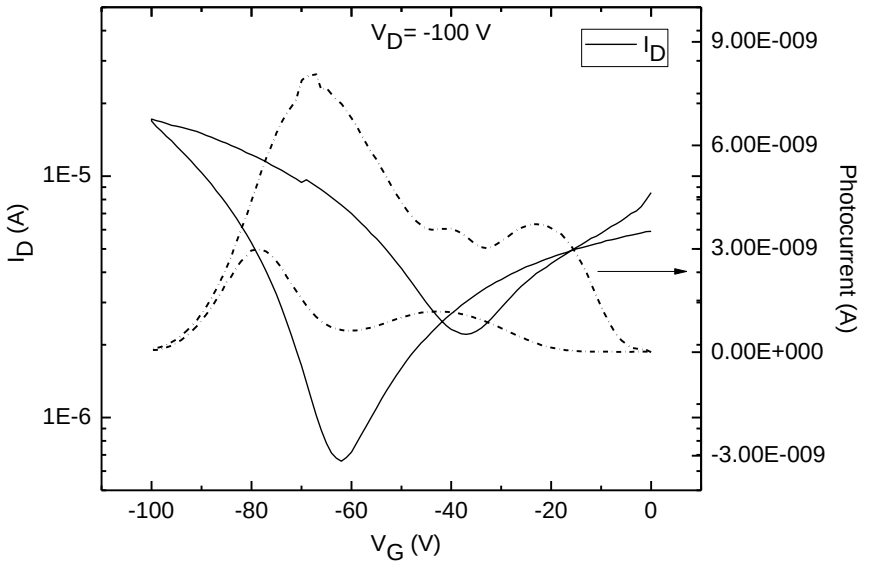

(a) Obtained photocurrent on F8BT-50$\mathring{A}$ TPP device during gate voltage sweep

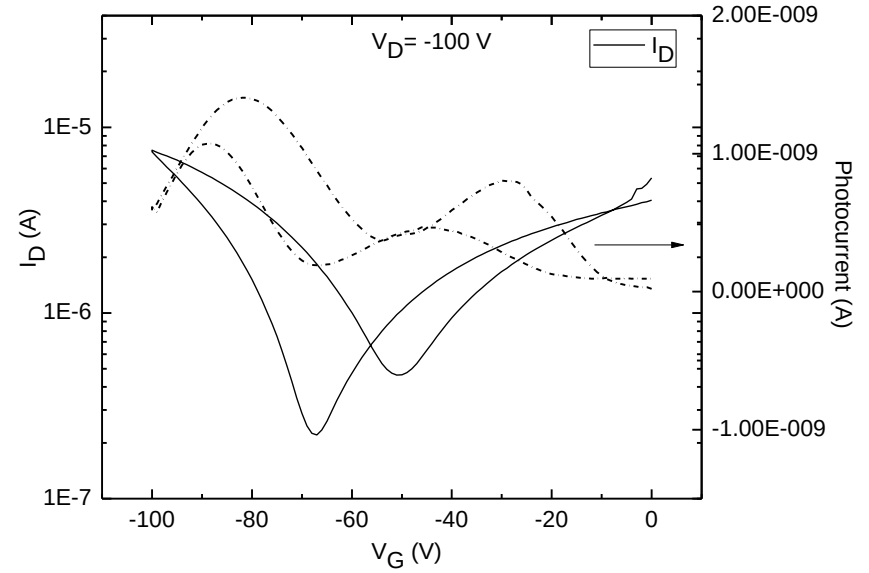

(b) Obtained photocurrent on F8BT-100$\mathring{A}$ TPP device during gate voltage sweep

Figure 46: Transfer curves and photocurrent measurement on different thickness of TPP films as a function of gate voltage

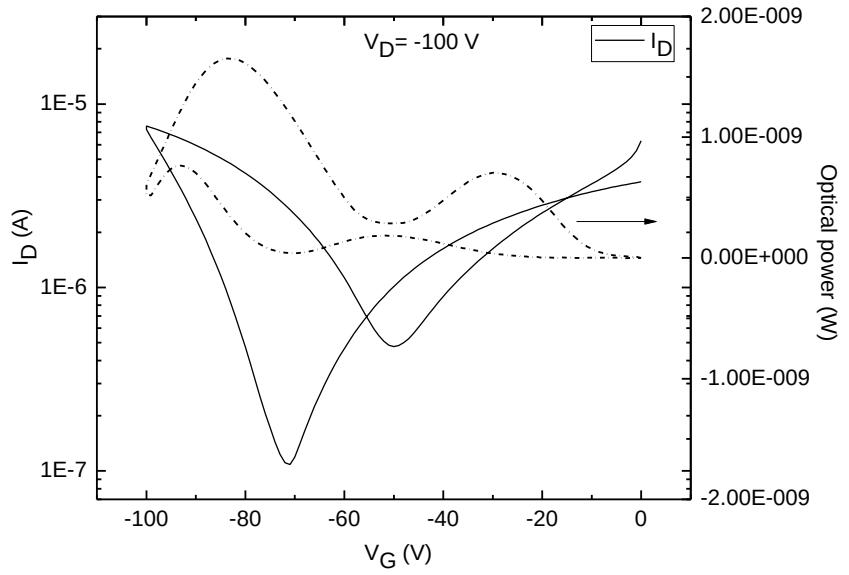

(a) Photocurrent measurement on 5 min baked device as a function of gate voltage

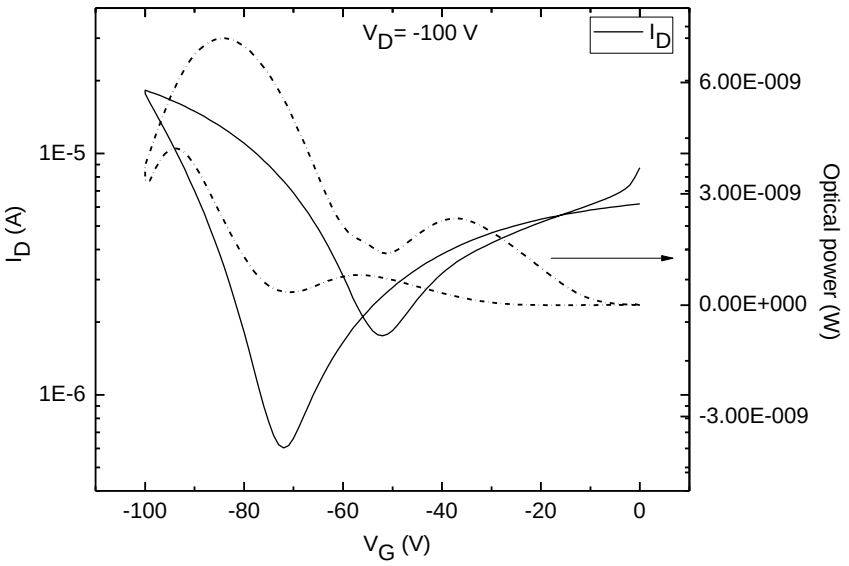

(b) Photocurrent measurement on 30 min baked device as a function of gate voltage

Figure 47: Transfer curve and photocurrent measurements on F8BT-70$\mathring{A}$ TPP device with different baking times

5.6.2 EQE Calculations

Based on measured photocurrent data, we can make a rough estimate of EQE in these F8BT-TPP devices. External Quantum Efficiency(EQE) is defined as the ratio of photons emitted to the number of injected charge carriers. As discussed previously, the light collected from photocurrent measurements is only a part of total number of photons emitted. Thus making an assumption that the collected light represents all the photons emitted and ignoring other losses is going to underestimate the actual efficiency in these devices. However, for the sake of the simplicity of the calculations it was assumed that there is no photon loss. The total amount of charge injected can be directly related the drain current in these devices.

To calculate EQE, photocurrent was first converted into optical power based on sensitivity of 818-ST photodetector at the peak wavelength. Optical power can be converted to the total number of photons based on the energy of photon at peak wavelength. Peak wavelength in these calculations was taken at 655nm corresponding to the stronger TPP peak in the optical spectra obtained. The drain current is converted into number of charges injected by dividing it by fundamental electron charge. The whole calculation thus yields EQE as a function of the voltage sweep. Fig.48 and fig.49 show the calculated EQE from the photocurrent measurements on thickness experiment and baking experiment respectively. Calculated EQE curve shows a distinct peak where the drain current is minimum and the device is working in ambipolar mode. It is expected that the light output efficiency will be maximum when both electrons and holes are present in the channel i.e.in the ambipolar region and the calculated EQE curves certainly justify the fact.

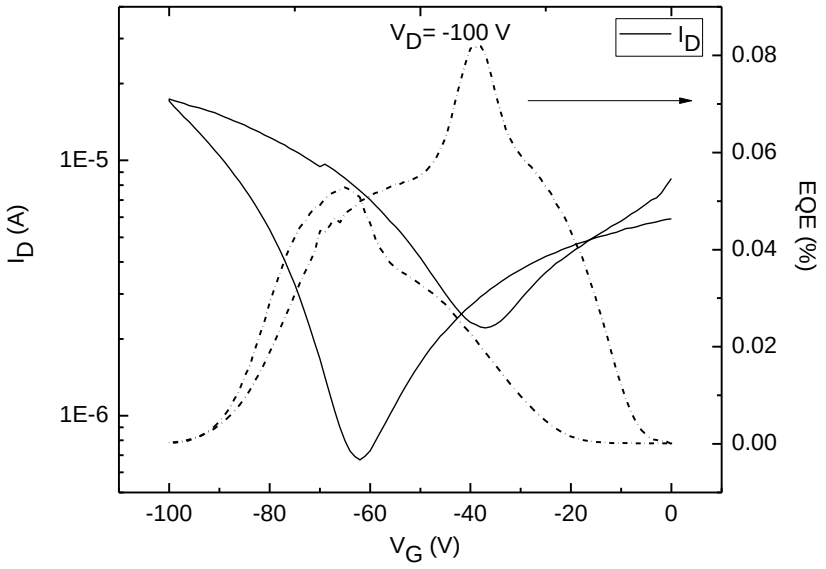

(a) Calculated EQE of F8BT-50$\mathring{A}$ TPP device

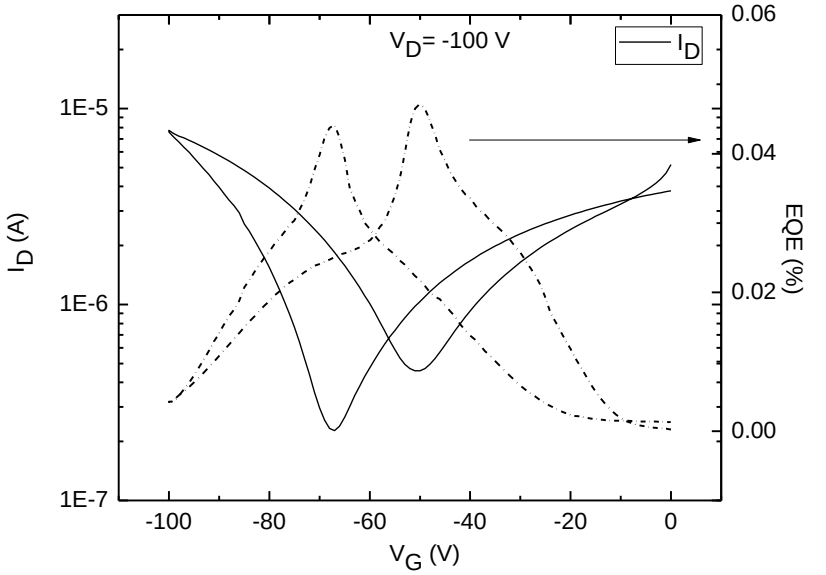

(b) Calculated EQE of F8BT-100$\mathring{A}$ TPP device

Figure 48: Transfer curves and calculated EQE on different thickness of TPP films as a function of gate voltage

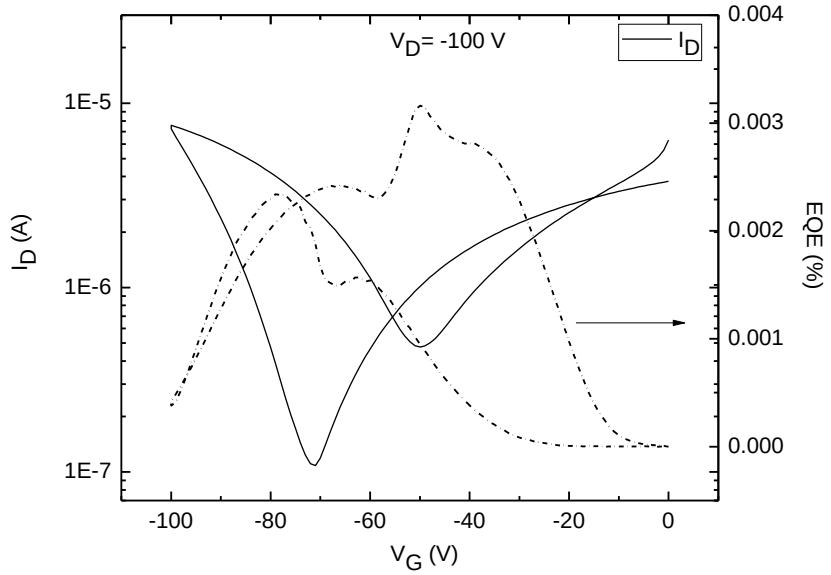

(a) Calculated EQE of 5 min baked device

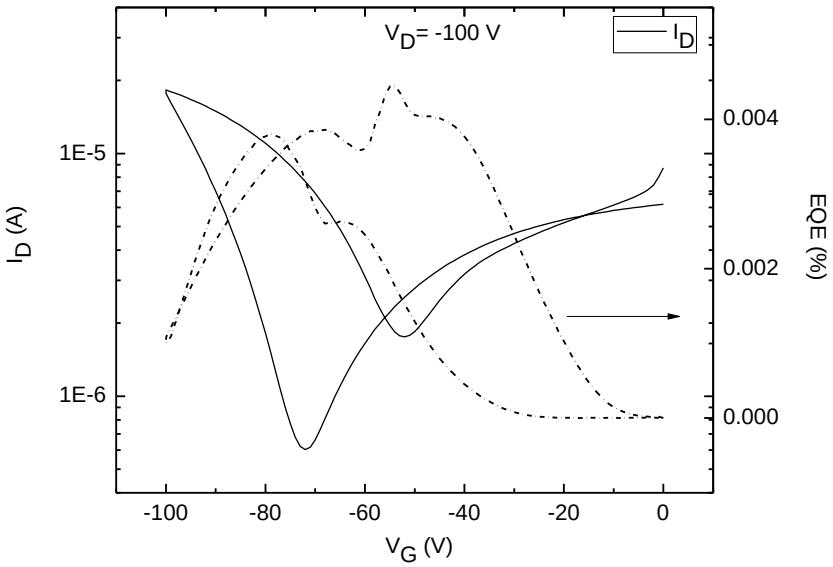

(b) Calculated EQE of 30 min baked device

Figure 49: Transfer curves and calculated EQE on F8BT-70$\mathring{A}$ TPP device with different baking times as a function of gate voltage

5.7 Conclusion

To summarize, we fabricated light emitting F8BT transistors in a top gate geometry with calculated mobility values comparable with the reported values. TPP was used as a dopant in F8BT devices in a modified bi-layer transistor architecture. TPP emission was identified in obtained EL spectra of transistors. Photocurrent measurements were performed as a function of gate voltage and EQE was calculated from these measurements.

References

[1] J. Zaumseil, C. Donley, J. Kim, R. Friend and H. Sirringhaus, Adv. Mater. (Weinheim, Ger.) **18** (2006).

[2] J. Zaumseil, C. R. McNeill, M. Bird, D. L. Smith, P. P. Ruden, M. Roberts, M. J. McKiernan, R. H. Friend and H. Sirringhaus, J. Appl. Phys. **103**, 064517 (2008).

[3] R. C. G. Naber, M. Bird and H. Sirringhaus, Appl. Phys. Lett. **93**, 023301 (2008).

[4] M. Schidleja, C. Melzer and H. von Seggern, Advanced Materials **21**, 1172 (2009).

[5] M. C. Gwinner, S. Khodabakhsh, H. Giessen and H. Sirringhaus, Chemistry of Materials **21**, 4425 (2009), [http://pubs.acs.org/doi/pdf/10.1021/cm900982a].

[6] J. S. Swensen, J. Yuen, D. Gargas, S. K. Buratto and A. Heeger, J. Appl. Phys. **102**, 013103 (2007).

[7] R. Capelli, S. Toffanin, G. Generali, H. Usta and A. F. . M. Muccini, Nature Materials **9**, 596 (2010).

[8] M. C. Gwinner, S. Khodabakhsh, M. H. Song, H. Schweizer, H. Giessen and H. Sirringhaus, Advanced Functional Materials **19**, 1360 (2009).

6 Future Work

OLETs can be considered as relatively newer area of interest amongst organic semiconductor devices. Current research on OLETs is focussed on developing new ways to fabricate transistors and generate efficient light emission. Over the part few years several materials and different strategies have been employed in order to achieve successful light emission. However, some questions still remain unanswered in terms of understanding the physics of OLETs and also develop a viable strategy to go towards electrically pumped organic lasers. Some of the things that should be tried in order to improve and understand OLETs better are outlined below.

6.1 BSBP Transistors

BSBP is an attractive host material to incorporate energy transfer into ambipolar OLETs because of its wide band gap and blue light emission. However, BSBP is not studied extensively in terms of its material properties. It is desirable to fully characterize BSBP before using it as host molecule in OLETs. BSBP transistors were fabricated using the material synthesized by our collaborators at University of Texas. This material was further purified by subliming and recrystallizing in a glass tube under flowing Ar gas. The transistors fabricated with raw BSBP did not work as ambipolar transistors.Transistors fabricated with purified BSBP worked as ambipolar transistors as shown in fig.50. Fig.50(a) shows transfer curve obtained on transistors fabricated with BSBP purified one time while fig.50(b) shows transfer characteristics of transistor fabricated with BSBP purified twice. As seen from the obtained transfer curves, the transfer properties improve with purification. Raw material consisted mixture of cis-trans isomers while purified material consists mainly of trans isomer. Based on preliminary NMR data we think that trans-trans conformation is stable conformer at high temperature and shows stable thermal evaporation and better ambipolar properties. This also agrees with the absorption and FTIR measurements performed on trans-trans isomer. However,more experiments are needed to establish the nature of isomers after purification. A thorough study should be performed on BSBP and its isomers involving XRD,PL and transistor measurements on BSBP.

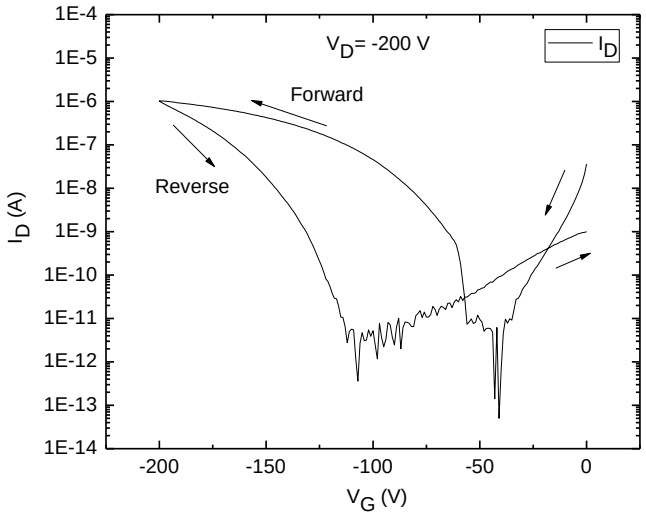

(a) Ambipolar transfer curves of transistors fabricated with BSBP purified 1 time

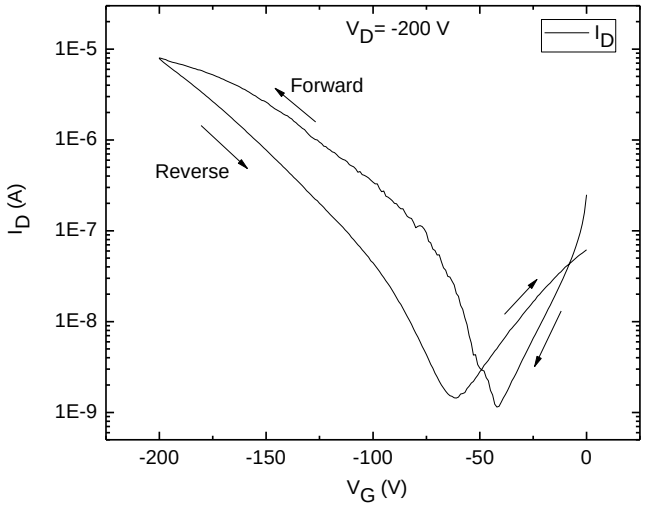

(b) Ambipolar transfer curves of transistors fabricated with BSBP purified 2 times

Figure 50: Transfer characteristics of BSBP transistors with extra purification of synthesized material

6.2 Modifying Device Architecture

We tried top gate-bottom contact and bottom gate-top contact architectures with Pentacene, BSBP and F8BT with symmetric contacts. As described in section 2.1.1 source-drain contacts are important for the injection of holes and electrons. It is necessary to align the energy levels of the source and drain electrodes to the HOMO and LUMO levels of the semiconductor in order to facilitate efficient charge injection. Using only one metal for both the source and drain electrodes (symmetric electrodes) makes only one of energy levels (HOMO or LUMO) closely aligned with metal work function for sufficiently large energy band gap semiconductor. If the HOMO and LUMO levels of the semiconductors are well aligned with source and drain electrode with the use of two different metals with suitable work functions, the chances of fabricating an ambipolar transistor are improved. In such a case one electrode acts as source of holes (e.g. Au, Ag) and the other electrode would be the source for electrons (e.g. Ca, Al).

Several research groups have utilized this idea of asymmetric electrodes effectively. Ambipolar pentacene transistor with Au and Ca contacts is reported.[1] Sakanoue et al[2] and Swensen et al[3] have used asymmetric contacts with ambipolar materials BSBP-C6 and Super Yellow, respectively. Recently, there have been reports of electroluminescence from Pentacene ambipolar transistors by using asymmetric Au and Ca contacts.[4] Similarly, to achieve better device performance in BSBP transistors asymmetric contacts should be employed. The effect of contacts should also be systematically analyzed by measuring contact resistance in BSBP ambipolar transistors.

OLETs in tri-layer geometry have been reported as viable alternative to conventional single material ambipolar OLETs.[9] However, working mechanism of these devices is still not completely understood. Different device architectures can be employed to systematically

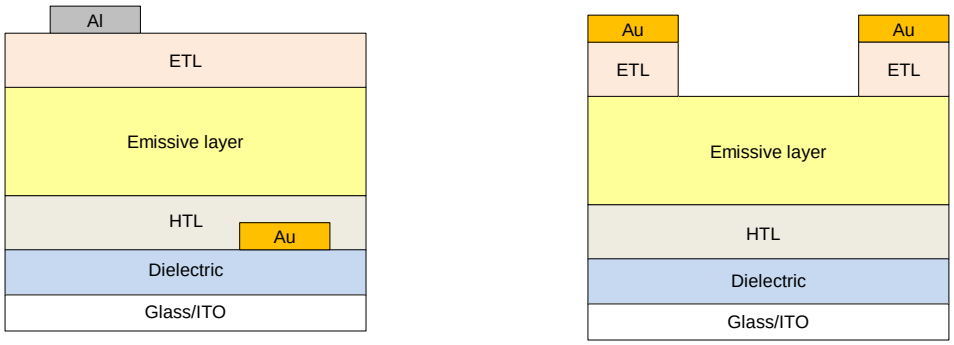

(a) Tri-layer transistor devices with staggered source and drain electrodes

(b) Tri-layer device with discontinuous top injection layer

Figure 51: Proposed variations of tri-layer device architectures

study tri-layer devices and also to optimize the device efficiencies. As shown in fig.51(a) a device with staggered contacts can be fabricated in order to improve charge carrier injection in these devices. Similarly, by having a discontinuous top injection layer as shown in fig.51(b) can be fabricated to collect more light from top without compromising charge injection. Along with these proposed device geometries, a systematic study of these devices should be performed by varying thicknesses of different layers including the dielectric. This will allow us to better characterize tri-layer devices as a function of device resistance and amount of charge injected.

6.3 Device modeling and Characterization

With the emergence of alternative tri-layer device structures along with conventional single material OLETs, its necessary to thoroughly analyze and understand the working of different device geometries. Working mechanism of tri-layer transistors is still not completely clear and both device modeling and transistor characterization measurements should throw more light on this issue.

Displacement current measurement is an attractive method to study the transient effects on organic semiconductor transistors as shown by Liang et al.[5] This method is a powerful tool to study different contacts and the involved induced charge densities in a transistor geometry. It can also elucidate to the amount of traps present at semiconductor-dielectric interface. The displacement current measurement on Pentacene transistors with PMMA dielectric and Aluminum contacts was performed by Liang et al[6]. Similarly, studying the contact effects and charge densities should be carried out for BSBP and other light emitting transistors. Similarly, contact resistance measurements should be performed on tri-layer transistors in order to understand the effect of contact resistance and device resistance.

Ambipolar OLETs have been modeled in order to simulate the drain current and the position of emission zone in the channel as a function of applied Gate and Drain voltage for Pentacene and F8BT transistors.[7] [8] Device modeling can serve as an important tool in order to understand tri-layer light emitting transistors and should be carried out. This will help in terms of selecting the right materials in an optimal geometry that will yield the best results in terms of light output and efficiency.

6.4 Energy Transfer in OLETs

Organic light emitting transistors have attracted a lot of attention since they were first demonstrated. This is mainly due the fact that they offer attractive option of combining OLEDs and transistors in one device and also because of their gate controlled light emission properties. Many researchers believe that the horizontal geometry of OLETs could be a viable option for getting towards electrically pumped organic laser systems. Thus, improving OLET device efficiencies is desired along with increase in exciton densities and light output.

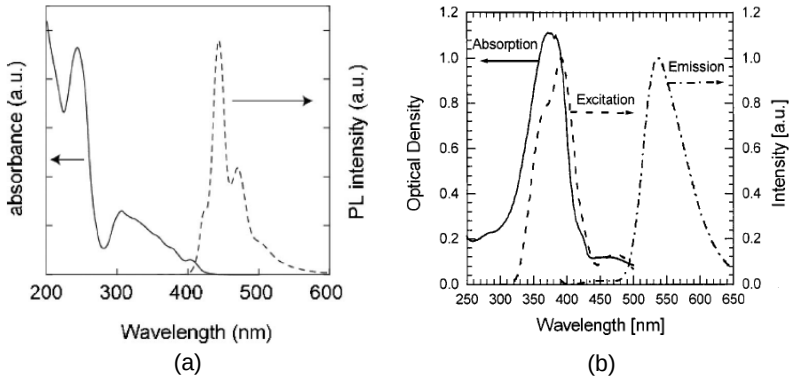

Figure 52: Emission spectrum of ambipolar light emitting molecules
(a) BSBP [11] and (b) F8BT [12]

Energy transfer from a suitable host material to a luminescent guest has played a major role in developing efficient OLED devices as discussed. The use of dopants separates the functions of charge transport and light emission on two different materials. Furthermore by using phosphorescent dopants we can effectively make use of triplet excited states formed on the host material. In principle, this same idea can then be used in ambipolar light emitting transistors. Energy transfer can also be used as a probe to understand the exact device physics of ambipolar OLETs. Although it is believed that hole and electron accumulation layers in OLET overlap to create excitons which then radiatively decay[3], the exact physics

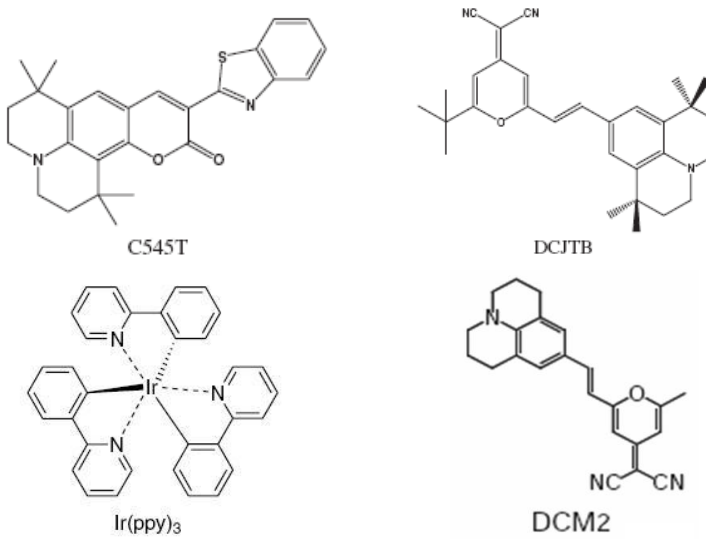

Figure 53: List of possible dopants to be used with BSBP and F8BT OLETs

of exciton formation and light emission is not thoroughly understood. With the help of luminescent dopants we can get further insights on this fundamental question. Figure 52 shows the emission spectrum of possible host ambipolar molecules. It is important that the absorption spectrum of this dopant has a significant overlap with the emission spectrum of ambipolar material to facilitate energy transfer. Figure 53 lists possible dopants that can potentially be used for efficient energy transfer in F8BT and BSBP OLETs.

This idea of energy transfer has been reported in a different vertical multi-layer OLET structure.[9]. Sirringhaus et al. have also incorporated a rib waveguide structure with F8BT light emitting device which might be a step towards getting electrically pumped OLET device.[10] Although TPP worked as a dopant in F8BT-TPP system, it is unclear how these devices work in a bi-layer geometry. Apart from TPP being soluble in n-butyl acetate its low PL efficiency in films is also one of the problems with this system. A red laser dye with high PL efficiency can serve as a viable option and should be incorporated

with F8BT OLETs and studied. Various red emitting efficient dopants have been reported in OLED literature. DCJTB and dyes like DCM2 can be used with F8BT in order to study energy transfer in OLETs. Some other host-guest combinations using BSBP as host are also listed.

Although several groups have reported the quantum efficiencies of ambipolar devices, a standard method which will take into account losses due to quenching and other non-radiative mechanisms has not been developed. The method of light collection through these devices is crucial in calculating efficiency of OLETs as there is light emission from a narrow line inside the channel and not the whole channel. Two methods that are employed to collect and measure light from OLEDs are use of a photodiode calibrated to measure the number of excitons generated and an integrating sphere arrangement. External quantum efficiency(EQE) for OLETs can be defined to be the ratio of number of photons emitted out from the top of the device to injected charge carriers.[17] The later quantity can be related to the drain current flowing through the channel[18] while photons out will contribute to photocurrent. While calculating the efficiencies it is assumed that all charge carriers in emission zone have recombined while effects like carrier quenching are not taken into account. Also, in case of F8BT devices it is assumed that semi-transparent Au gate doesn't absorb any of the generated excitons.[19] It is thus important that different loss and quenching mechanisms should first be understood in order to improve quantum efficiency calculations in OLETs.

References

[1] R. Schmechel, M. Ahles and H. von Seggern, J. Appl. Phys. **98**, 084511 (2005).

[2] T. Sakanoue, M. Yahiro, C. Adachi, J. H. Burroughes, Y. Oku, N. Shimoji, T. Takahashi and A. Toshimitsu, Appl. Phys. Lett. **92**, 053505 (2008).

[3] J. S. Swensen, J. Yuen, D. Gargas, S. K. Buratto and A. Heeger, J. Appl. Phys. **102**, 013103 (2007).

[4] M. Schidleja, C. Melzer and H. von Seggern, Appl. Phys. Lett. **94**, 123307 (2009).

[5] Y. Liang, C. D. Frisbie, H.-C. Chang and P. P. Ruden, Jour. Appl. Phys. **105**, 024514 (2009).

[6] L. Yan, *Examination of transient carrier behaviors in organic field-effect devices via displacement current measurement*, PhD thesis, University of Minnesota, Jan 2011.

[7] M. Schidleja, C. Melzer and heinz von Seggern, Frequenz **62**, 100 (2008).

[8] D. L. Smith and P. P. Ruden, Appl. Phys. Lett. **89**, 233519 (2006).

[9] R. Capelli, S. Toffanin, G. Generali, H. Usta and A. F. . M. Muccini, Nature Materials **9**, 596 (2010).

[10] M. C. Gwinner, S. Khodabakhsh, M. H. Song, H. Schweizer, H. Giessen and H. Sirringhaus, Advanced Functional Materials **19**, 1360 (2009).

[11] T. Sakanoue, M. Yahiro, C. Adachi, H. Uchiuzou, T. Takahashi and A. Toshimita, Appl. Phys. Lett. **90**, 171118 (2007).

[12] M. Stoessel, G. Wittmann, J. Staudigel, F. Steuber, J. B. ssing, W. Roth, H. Klausmann, W. Rogler, J. Simmerer, A. Winnacker, M. Inbasekaran and E. P. Woo, J. Appl. Phys. **87**, 4467 (2000).

[13] T. Tsuboia and M. Tanigawab, Thin Solid Films **438-439**, 301 (2003).

[14] C.-C. Lee, M.-Y. Chang, P.-T. Huang, Y. C. Chen, , Y. Chang and S.-W. Liu, J. Appl. Phys. **101**, 114501 (2007).

[15] C.-C. Tsou, H.-T. Lu and M. Yokoyama, Solid-State Electron. **49**, 1595 (2005).

[16] Y.-S. Yao, Q.-X. Zhou, X.-S. Wang, Y. Wang, and B.-W. Zhang, Adv. Funct. Mater. **17**, 93 (2007).

[17] R. Capelli, F. Dinelli, S. Toffanin, F. Todescato, M. Murgia, M. Muccini, A. Facchetti and T. J. Marks, Journal of Physical Chemistry **112**, 12993 (2008).

[18] E. B. Namdas, P. Ledochowitsch, J. D. Yuen, D. Moses and A. Heeger, Appl. Phys. Lett. **92**, 183304 (2008).

[19] J. Zaumseil, C. R. McNeill, M. Bird, D. L. Smith, P. P. Ruden, M. Roberts, M. J. McKiernan, R. H. Friend and H. Sirringhaus, J. Appl. Phys. **103**, 064517 (2008).